UNIVERSIDADE
BEIRA INTERIOR

Optimal and Robust Control of Atmospheric Reentry Trajectories

(Versão corrigida após defesa)

António Miguel Peralta Moreira

Dissertação para obtenção do Grau de Mestre em

Engenharia Aeronáutica

(Mestrado Integrado)

Orientador: Professor Doutor Kouamana Bousson

abril de 2022

Dedicated to my Family

Acknowledgments

I am thankful for all the support that I received from Dr. Kouamana Bousson throughout all phases of this dissertation and for bringing this subject to me. The application of the H_∞ was surely a difficult and defying task, which gave me mathematical and programming skills that I would not have in another type of dissertation. I deeply appreciate the help on the simplification and explanation of the mathematical procedure behind H_∞, which without help would reveal to be an even harder job.

I would also like to appreciate all the support that I had from my mother, my brother, and my father, who helped me academically and financially through all my years at the University of Beira Interior and made it possible for me to study and achieve my dream of becoming an Aeronautical Engineer. I was lucky to have them at my side, helping me succeed in every step of the way.

I would also like to thank all my friends that I had the luck to have throughout this Master's Degree. The nights of studying until the sun rose, the nights of fun that we had in the beautiful city of Covilhã, the stories that we shared through the years, and all the moments we shared will forever remain in my memory. You have all taught me to be a better person every day and I happily owe part of who I am to you.

For those who have shared a home with me - Gonçalo Luís, Viktor Zombori, André Rodrigues, and Filipe Senra - I give a special thanks for being there for me at the heaviest of times and for sharing the craziest and funny stories with me; to Tiago Morão, for being a special friend and a teacher more patient than any other; and to my girlfriend Francisca Serras, who was solely responsible for encouraging me to never give up and to fight until the very end of this degree, even at the most difficult phases of this dissertation. Thank you all.

Resumo

A reentrada na atmosfera terrestre é uma das fases mais difíceis da missão de qualquer nave espacial. Durante a reentrada, seguir uma trajectória óptima em termos de taxa mínima de aquecimento, pressão dinâmica e maáxima desaceleração é vital para o sucesso da missão. Esta dissertação propõe o design de um controlador baseado em métodos de H_∞, com o objectivo de alcançar um controlo óptimo e robusto para um Veículo de Reentrada na atmosfera capaz de produzir sustentação.

Esta dissertação começa com um resumo da teoria e história por detrás do Programa Espacial do Vaivém, incluindo o planeamento de trajectórias e descrições do Modelo de Dinâmica de Voo de Reentrada. A análise da trajectória de referência obtida seguir-se-á e será feita a sua comparação com uma trajectória real do vaivém. A concepção e configuração do controlador H_∞ virá depois, começando com a linearização do sistema obtida no passo anterior e terminando com o recálculo das variáveis de estado do veículo após a sua aplicação. A perturbação é então aplicada e os resultados do accionamento do controlador são exibidos. O controlador H_∞ para Veículo de Reentrada capaz de produzir Sustentação mostrou ser uma aplicação útil apresentando resultados satisfatórios e significativos nesta fase crítica de voo.

Palavras-Chave

Controlo Ótimo e Robusto — Veículo de Reentrada — Método de Controlo H_∞

Abstract

Reentering the Earth's atmosphere is one of the most difficult phases of any spaceship's mission. During reentry, following an optimal trajectory in terms of minimal heating rate, dynamic pressure, and maximum deceleration is vital to the mission's success. This dissertation proposes a novel design for a controller based on H_∞ control methods, with the goal of achieving optimal and robust control for a Reentry Lifting Vehicle.

This dissertation begins by summarizing the theory and history behind the Shuttle Space Program, including the planning of its trajectories and descriptions of the Reentry Flight Dynamics Model. The analysis of the obtained reference trajectory will follow and the comparison of it to a real shuttle trajectory will be made. The design and configuration of the H_∞ controller comes after, beginning with the linearization of the obtained system in the previous step and ending with the recalculation of vehicle state variables after its application. The disturbance is then applied and the results of the actuation of the controller are displayed. The H_∞ controller for Reentry Lifting Vehicle proves itself to be a useful application presenting satisfying and significant results in this critical phase of flight.

Keywords

Optimal and Robust Control — Reentry Lifting Vehicle — H_∞ Control Method

Contents

List of Figures

List of Tables

List of Acronyms

3DOF	Three-Degree-Of-Freedom
AOA	Abort Once Around
AoA	Angle of Attack
ARE	Algebraic Riccati Equation
ATO	Abort To Orbit
COM	Center Of Motion
KSC	Kennedy Space Center
LQR	Linear Quadratic Regulator
NASA	National Aeronautics and Space Administration
RLV	Reentry Lifting Vehicle
RTLS	Return To Launch Site
STS	Space Transportation System
TAEM	Target Area Energy Management
TLA	Transatlantic Landing Abort
TPS	Temperature Protective Shield

List of Symbols

Symbol	Description	Units
$\dot{Q}_s$	Heating Rate	$[W/m^2]$
$\bar{x}(t)$	Integrated State Vector	[-]
$\bar{u}(t)$	Integrated Control Vector	[-]
α	Angle of Attack	$[deg]$ or $[rad]$
β	Drifting Angle	$[deg]$ or $[rad]$
δ_e	Elevator's Deflection	$[deg]$
ζ	Disturbance Matrix	[-]
θ	Longitude	$[deg]$ or $[rad]$
λ	Pith Angle	$[deg]$
μ	Disturbance Attenuation	[-]
ρ	Air Density	$[kg/m^3]$
σ	Bank Angle	$[deg]$ or $[rad]$
ϕ	Latitude	$[deg]$ or $[rad]$
ψ	Heading Angle	$[deg]$ or $[rad]$
γ	Flight Path Angle	$[deg]$ or $[rad]$
ω	Atmospheric Scale Height	$[m^-1]$
A	State Matrix	[-]
a	Deceleration	$[m/s^2]$
B	Control Matrix	[-]
BC	Ballistic Coefficient	$[kg/m^2]$
$\bar{c}$	Medium Chord	$[m]$
C_L	Aerodynamic Lift Coefficient	[-]
C_D	Aerodynamic Drag Coefficient	[-]
D	Aerodynamic Drag	$[N]$
E	Output Matrix	[-]
e	Base of the Natural Algorithm	[-]
g	Earth's Gravitational Acceleration	$[m/s^2]$
h	Altitude	$[m]$
h_s	Scalar Height Coefficient	$[m]$
J	Objective Function	[-]
K	Feedback Gain Matrix	[-]
k_Q	Heating Rate Normalization Constant	$[\sqrt{kg/m}]$
L	Aerodynamic Lift	$[N]$
M	Matrix of Extracted Julia State Variables	[-]
m	Estimated Mass	$[kg]$

Symbol	Description	Units
M_a	Mach Number	[-]
N	Matrix of Extracted Julia Control Variables	[-]
N_{T_j}	Matrix of Extracted Julia Control Variables for $\gamma_i = -1, 1^{\circ}$	[-]
N_{Z_j}	Matrix of Extracted Julia Control Variables for $\gamma_i = -5^{\circ}$	[-]
P	Plant Matrix	[-]
Q	State Weighting Matrix	[-]
$Q_{intensity}$	Intensity of State Weighting Matrix	[-]
q	Dynamic Pressure	$[Pa]$
q_p	Pitch Rate	$[deg/s]$
R	Control Weighting Matrix	[-]
R_0	Earth's Medium Radius	$[m]$
r	Distance Between Earth's COM and the RLV's COM	$[m]$
r_{nose}	Vehicle Nose Radius	$[m]$
S	Vehicle Sectional Area	$[m^2]$
T_j	Matrix of Extracted Julia State Variables for $\gamma_i = -1, 1^{\circ}$	[-]
t	Time	$[s]$
t_s	Time Step	$[s]$
$u(t)$	Control Vector	[-]
v	Velocity	$[m/s]$
X, Y, Z	Relative Position Components	$[m]$
$x(t)$	State Vector	[-]
$y(t)$	Output Vector	[-]
Z_j	Matrix of Extracted Julia State Variables for $\gamma_i = -5^{\circ}$	[-]

Chapter 1

Introduction

Adventuring into space has been for a long time an accomplished dream of mankind. However, humanity will never stop exploring beyond the limits of our planet's atmosphere. While exiting the atmosphere is itself a challenge, being capable of safely landing and reentering the atmosphere with a manned space aircraft is an even heavier challenge.

Throughout the years, numerous satellites have been launched into the atmosphere with no plan of return, becoming sooner or later disposable material continuously in orbit. Guaranteeing the safe return of the no-longer-used satellites and spacecraft is a critical mission if we want to leave our atmosphere as clean as possible. According to *Portugal Space*: "every year approximately 100 tons of uncontrolled debris reenter Earth's atmosphere, a situation that explains the urgency of developing technology and solutions that allow the controlled and safe removal of the debris humanity left in space" [1].

Reentering the atmosphere is then the most critical part of the mission of a shuttle or any similar spaceship. From an astronaut's point of view, the atmosphere presents a dense fluid, which at orbital velocities, is not that far from the surface of a lake [2]. In this dissertation, the Reentry Lifting Vehicle (RLV) used for the development of the controller will be the model of a shuttle.

The trajectory followed to begin the process of reentering the atmosphere must begin with a small flight path angle - γ - between $1,1^\circ$ and $1,5^\circ$ and a precise speed [3]. If the γ is smaller than $1,1^\circ$, the vehicle may not entry the atmosphere and drive off again into the cold space. On the other hand, if γ is bigger than $1,5^\circ$ the vehicle can have a fiery and tragic ending if it doesn't correct its trajectory. In the middle of these two situations, we find the correct trajectory for the RLV.

The trajectory followed must allow the minimum temperature peaks considering the aerodynamic heating along the way to ensure the integrity of the shuttle and no loss of materials during the reentry. Choosing the ideal systems that can withstand these temperatures is preeminent to ensure the maneuverability of the vehicle. The tragedy of Columbia (STS-107) is a fatal reminder of the dangerous thermal and aerodynamic environment that any vehicle reentering the atmosphere endures [3].

Given the importance of following a reentry reference trajectory, a control system that ensures the RLV continuously follows it becomes essential.

1.1 Planning the reentry trajectory

The design and calculation of the reentry trajectory can be summarized in 3 competing requirements: deceleration limits, heating limits, and impact/landing accuracy [4].

The materials used in the vehicle directly impact the maximum deceleration it can endure. Considering g as a deceleration unit and g being the gravitational acceleration at sea level ($9,80665\ m/s^2$), materials like steel can only endure a certain amount of g until they fold like paper. Nevertheless, the materials used in these vehicles can withstand hundreds of g's if correctly sized and manufactured. However, the human species can only withstand a maximum deceleration of $12\ g$'s [2].

The heating is also a noticeable problem. The friction between the air and the RLV traveling at thousands of meters per second drastically increases the temperature of its materials. In other words, the kinetic energy is being transformed into heat during the reentry phase of the shuttle. We must study the normal temperature throughout the reentry as well as the peak temperature of the shuttle, which can reach values of $1648°C$ [5].

The last requirement to consider is the accuracy of lading or impact. This component is determined according to the type of mission. For example, the accuracy of a crashing satellite, regardless of its importance, may not be as demanding as the accuracy of a missile warhead. On the other hand, the velocity of the impact of a missile will be a less important factor than in a case of a reentering shuttle, where the final velocity is certainly an important one.

Deciding how much influence will each requirement have on the trajectory chosen is part of the designing process. For a given problem the requirements previously explained will have a certain weight to the calculations of trajectory, following the mission's nature.

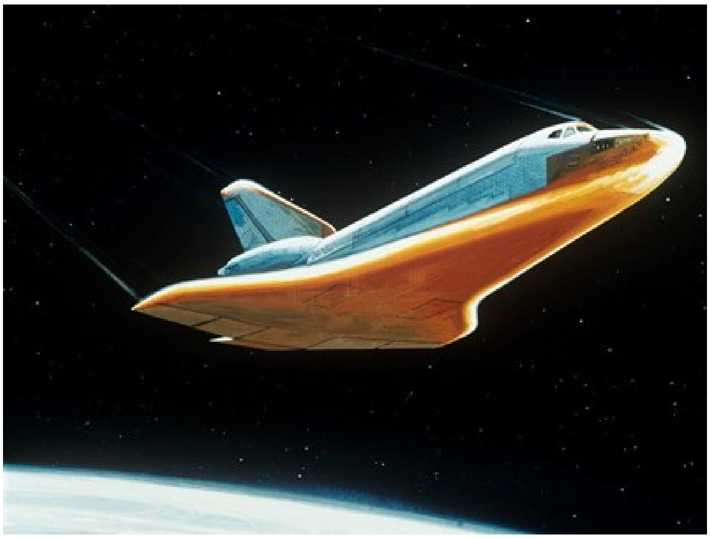

Figure 1.1: Artist Impression of a shuttle during reentry, by NASA/Science photo library.

1.2 The importance of a Temperature Protective Shield (TPS)

In this subsection, we will continue to follow the knowledge shared by the National Aeronautics and Space Administration - NASA - [6, 7] explaining why the TPS is an essential part of the RLV.

As mentioned before, the surface temperature of the RLV may reach or even surpass values of $1648°C$. The RLV will need a protective shield dedicated to isolating the inner layers of metal of the vehicle and the life inside if the case applies. The TPS must also guarantee the well-being of the control and monitor systems throughout all the reentry mission phases, ensuring the maneuverability of the RLV especially at critical stages of flight.

The materials used in the TPS must also endure forces due to deflection caused by temperature variations it suffers, given the fact that the RLV is not only subjected to substantial heat during reentry but also to extremely negative temperatures of -$156°C$ when it travels through cold space.

Additionally, the TPS must be capable of protecting the RLV even when abort situations occur, drastically increasing temperature to a peak level provoking high deflections and stress inside the TPS inner layers. Examples of these abort missions could be found in [8]:

- *Abort To Orbit* (ATO), where the vehicle can temporarily achieve an orbit that is lower than the nominal orbit. This mode allows for the crew to evaluate possible existing problems and decide whether to return to Kennedy Space Center (KSC) or to raise the orbit and continue the mission;

- *Abort Once Around* (AOA), designed to allow the shuttle to go around Earth one time and make a normal entry and landing;

- *Return To Launch Site* (RTLS), where the shuttle returned to the KSC approximately 25 minutes after lift-off and after the dissipation of propellant;

- *Transatlantic Landing Abort* (TLA), when the return to the KSC reveals itself impossible and the shuttle will land on the other side of the Atlantic Ocean, being the trajectory a ballistic one not requiring the use of an orbital maneuvering system maneuver.

To enhance the knowledge on the possible abort situations that can occur, the fig. (1.2) is displayed:

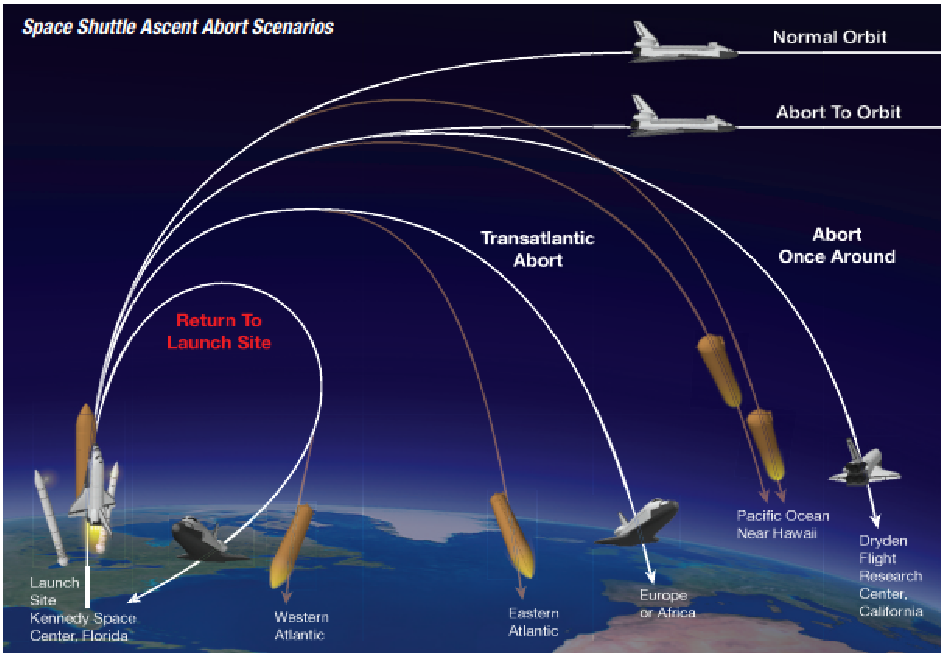

Figure 1.2: Space Shuttle Ascent Abort Scenarios. [6]

The TPS is then composed of several materials as reinforced carbon-carbon, flexible reusable surface insulation, and ceramic tiles which would be those who can endure the highest temperatures of all. It was also important to guarantee a high emissivity throughout all coatings to guarantee the maximum rejection of incoming convective heat through the radioactive heat transfer, as explained in [6].

The application of these TPS around the space shuttle can be observed in the following image, where we can see the tiles providing a smooth, aerodynamic surface while performing its role of protection. Different categories of TPS are used across the body of the RLV given the fact that the temperature heating peaks differ according to the zone of the vehicle being studied, and the need to always get the lightest and cheapest viable option naturally exists. Another impressive factor NASA has achieved with these TPS is the fact that they are reusable.

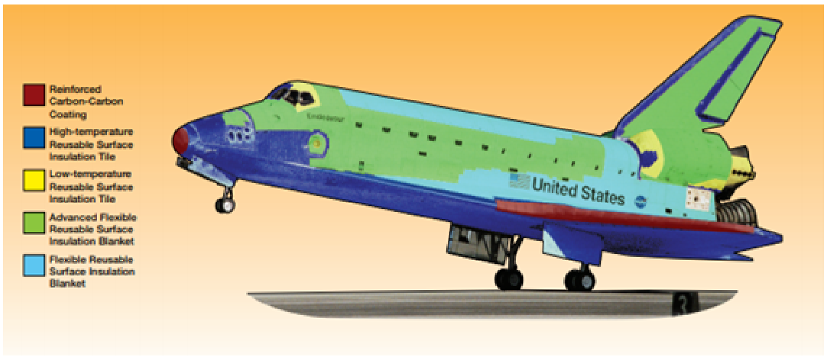
🟥 Reinforced Carbon-Carbon Coating
🟦 High-temperature Reusable Surface Insulation Tile
🟨 Low-temperature Reusable Surface Insulation Tile
🟩 Advanced Flexible Reusable Surface Insulation Blanket
🟦 Flexible Reusable Surface Insulation Blanket
United States

Figure 1.3: Orbiter's Temperature Protective Shield. [6]

1.3 Ballistic Reentry

There are two types of reentry trajectories, ballistic and lifting ones. The first case will be analyzed in this subsection while the second one will be addressed in the next subsection.

This trajectory occurs when the vehicle is subject to no aerodynamic force besides the aerodynamic drag, which means the vehicle never produces lift force throughout all phases of reentry ($C_L = 0$ and $L = 0$).

In these trajectories, the most important element to control is the ballistic coefficient BC, which following [2, 3, 9] is calculated by:

$$BC = \frac{m}{C_D S} \tag{1.1}$$

where m is the vehicle mass, C_D is the drag coefficient, and S is the reference area of the reentry vehicle. The ballistic coefficient is the most important factor in this kind of trajectory, as the heating and deceleration are less intense with a low BC value (low weight and/or high drag and large frontal area) and for a bigger value of BC the opposite occurs.

The vehicles that do this type of reentry are blunt ones like capsules or missiles with naturally no generation of lift and given its speed of descent, the need for a powerful temperature protective shield naturally surges.

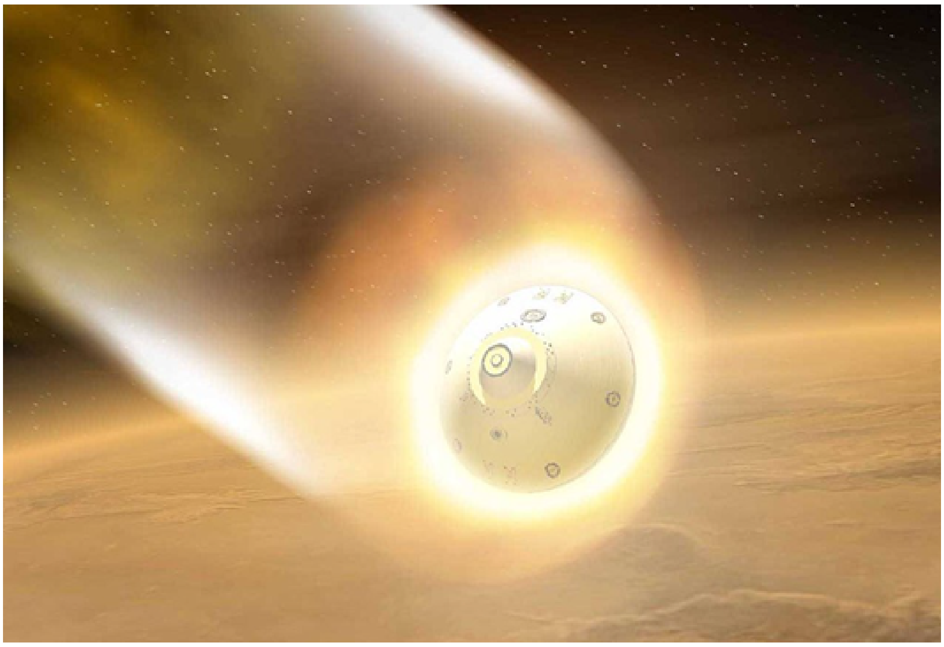

Figure 1.4: Artist Impression of Mars Exploration Rover.

Although this type of reentry exists and is still very important to study (for example the missile's accuracy is of tremendous importance given the need to produce minimal civilian casualties), the objective of this dissertation is to develop an optimal and robust controller for a RLV (where lift is produced) so this reentry trajectory will not be the one followed.

1.4 Lifting Reentry - A view over a typical shuttle reentry

For this section, we will consider a shuttle orbiting around Earth and how can we ensure its reentry, each step of the way.

The reentry corridor is the width on which the possible reentry trajectories are found due to the facts described in the following subsection.

1.4.1 Entry Corridor

One of the most recognized methods to plan the reentry trajectory of a RLV is the Entry Corridor. To use this method, information of the mission is needed, as the Vehicle speed Approach v_i and the flight path angle γ_i at a certain distance r_i.

For a RLV with a given ballistic coefficient, we can find two different constraints that limit the corridor. The constraint on which the deceleration and heating rate is impossible to withstand, being that from the crew or the vehicle, and the constraint on which the vehicle will not initiate the reentry phase due to the small gravitational force encountered when compared to the momentum of the vehicle. The first constraint is the undershoot, and the second the overshoot, as explained and summarized in [10].

The Entry Corridor can be defined by the region between the two constraints that create it, the undershoot and the overshoot.

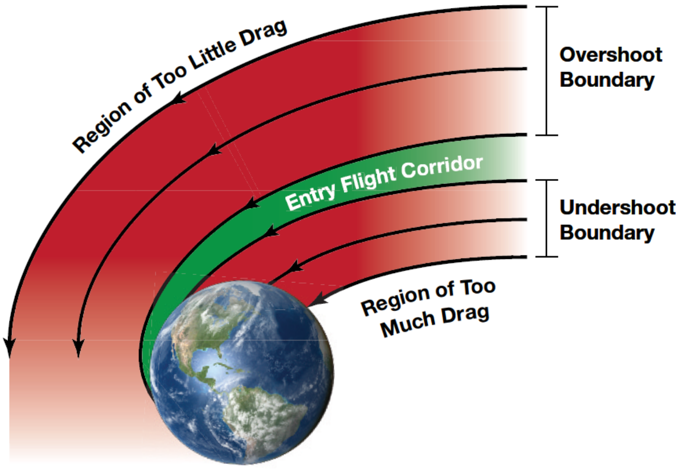

Figure 1.5: The reentry corridor. [10]

Flights from circular or elliptical orbits can recover when the trajectory is *undershooted* by an application of thrust at a large distance before initializing the reentry process.

On the other hand, if the given vehicle is at hypersonic velocity at an overshoot or undershoot trajectory, the guidance control is highly critical. For an undershoot trajectory the fuel needed to correct the trajectory could be less than required. An overshoot trajectory at this speed would also be difficult to correct, the vehicle would continue into the cold of space or in a highly elliptic ejection, resulting in a considerable amount of time until its return [4].

This method will allow adding more constraints to our problem to further achieve a better precision regarding the entry trajectory of the RLV. To give a greater insight on the problem at hand, the shuttle's orbiting speed is about $28.000\ km/h$ - it critically needs to lose a lot of speed to land on a specific runway and at a certain rate, so it doesn't melt when descending through the atmosphere. Safely losing all this speed is the key to this mission.

The beginning of the reentry phase consists of the exit of the shuttle's current orbit. To do so, the shuttle activates its maneuvering thrust engines, losing some of its speed and slowly leaving its orbit. This way the shuttle will slowly start falling towards the earth's atmosphere.

Since the shuttle is still at an overwhelming speed, it is necessary to take advantage of the drag force presented once it starts entering Earth's atmosphere.

1.4.2 Use of angle of attack (AoA)

With the shuttle now off the orbit, it needs to rotate itself to a certain AoA depending on the version of the shuttle being studied, maintaining this angle of attack throughout its descent [6]. The reason behind this is the urgent need for deceleration of the shuttle, and by maintaining a certain AoA the shuttle produces enough drag to start the deceleration while its temperature is possible to endure with its TPS.

In other words, if the AoA is smaller than the calculated value, the amount of drag produced would not be enough to decelerate the shuttle. While on the other hand with the angle of attack bigger than the same value the thermal energy produced by the friction between Earth's atmosphere and the shuttle would raise the temperature to a point where the TPS would not endure.

There is, however, a certain interval on which the angle of attack can variate, which is -3° to +3° from the needed AoA.

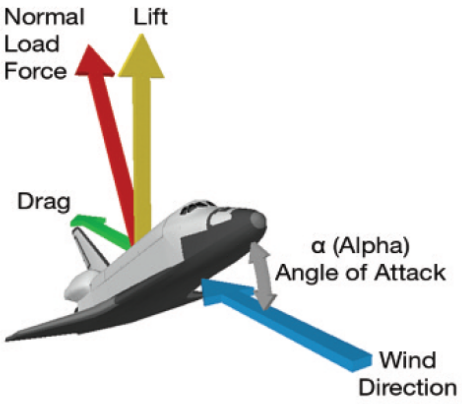

Figure 1.6: Representation of the shuttle's angle of attack during reentry. [6]

1.4.3 Use of Bank Angle

While descending with an AoA that produces considerable deceleration, aerodynamic lift (L) is also produced. As the altitude of the shuttle drops, Earth's atmosphere becomes denser and the lift produced is sufficient to impede the shuttle's reentry into the atmosphere [6].

The solution found to solve this problem was the use of the bank angle, maintaining the angle of attack. The bank angle is the angle made between the longitudinal axis of the shuttle and the vertical axis. By varying this angle, the vertical vector of lift becomes smaller than in the initial case allowing the shuttle to continue its decrease in altitude. On the other hand, the alteration of the bank angle will make the shuttle turn in the direction he is changing but has will be shown in fig. (1.7), it is constantly being monitored to change in the opposite direction to ensure its landing on the desired runway.

The bank angle can also be used to control how much deceleration is still needed to enter the final phase where the pilots take full command of the shuttle and prepare for landing. If we use a steeper bank angle, more deceleration is produced, and vice-versa.

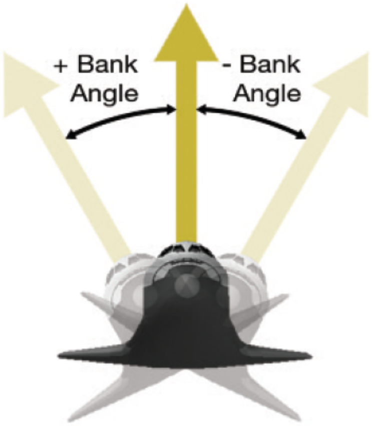

Figure 1.7: Representation of the shuttle's bank angle. [6]

Finally, the shuttle will have reached the velocity needed to start preparing its landing and its angle of attack can now decrease. This phase is called TAEM – *Target Area Energy Management* – which is not related in terms of control or maneuvers with the trajectory of reentry being studied. This phase will then not be included in this thesis since it is where manual control from the shuttle's pilots takes place. The controller produced will only be responsible for the trajectory of reentry until this phase has begun.

1.5 Common Assumptions Made

In this section the possible assumptions that can be made when we estimate the optimal trajectory of reentry will be discussed. Each assumption made will have a significant impact on the final result of the problem.

In the last ten years, many researchers have investigated new strategies to quickly generate a feasible and complete three-degree-of-freedom (3DOF) reentry reference trajectory for hypersonic vehicles [11].

Given the high processing power needed to calculate the trajectory of reentry most of the calculations are done on land and preloaded into the hypersonic vehicle before its take-off [11].

One of the most important assumptions made is the use of the spherical model of the Earth in the calculations of the reentry trajectory. It is a known factor that Earth has an elliptical form which can be observed by the cross-section of all the meridians. However, the benefits obtained by considering the Earth as a spherical body significantly justify the precision lost in the procedure as was made in [12, 13, 14].

Regarding Earth's rotation, there are two decisions that can be made: consider earth as a rotating body or as a stationary body. Considering the Earth's rotation as part of the equations, despite adding slightly more precision to the final results the outstanding difference in algorithm complexity makes the decision of considering the Earth as a stationary Body a viable decision, as was used in [14, 15, 16]. It would also require the monitoring of the inclination of trajectory to the equator at all times.

With these facts in mind, the method followed in this dissertation was the spherical non-rotating Earth.

Figure 1.8: Earth as a Spherical Model [17].

1.6 State of Art

As stated previously, establishing a reference reentry trajectory that ensures the integrity of the RLV throughout its descend presents a difficult challenge. For many years researchers have been looking for an optimal constrained reentry for hypersonic vehicles as stated in [11].

The development of a controller that ensures the RLV follows such a trajectory becomes a crucial task. Throughout the years, researchers have been looking for ways to develop a control system capable of stabilizing the RLV, returning it to the reference trajectory regardless of the disturbances suffered during its descend.

Marwan Bikdash et al. designed a fuzzy guidance for the shuttle orbiter during atmospheric reentry [18]. In it, the authors designed the reference trajectory using a drag-acceleration vs velocity profile. Making use of *Sugeno* approximations, the authors trained hybrid fuzzy-crisp interference systems with examples of past reentries. Moreover they utilized the surface-tracking guidance to alter the reference trajectory if there where severe disturbances affecting it. The algorithm was capable of stabilizing the RLV and alter the reference trajectory in the shown cases.

A predictor-corrector reentry guidance was proposed by Xiaoping Guo et al. in [19] based on Feedback Linearization to reduce the difference between reference trajectory and the RLV current state after an applied disturbance. The authors used the Quasi Equilibrium Glide Condition as another constraint and controlled the vehicle with the same control variables as in this dissertation - α and σ.

Another Predictive Controller was designed by Tao Ye et al in [20]. In this paper, the authors first designed the reference trajectory using nominal trajectory guidance method. The predictive control was developed using Gaussian pseudospectral method and the vehicle is subjected to disturbances to verify the controller's efficiency. The controller was capable of guiding the vehicle even when subject to external disturbances. However, the disturbances imposed were not of the same magnitude as the disturbances presented in this dissertation.

M. H. Breitner made use of *Rufus Philip Isaacs* nonlinear first-order partial differential equations to set up interior and boundary conditions, being the restrictions to the RLV similar to this dissertation [21]. Then, using neural networks and a multiple shooting method, the author produced a robust optimal guider for the RLV throughout its descent. The algorithm presented satisfying results and proved real-life applicability in its theory and numerical methods.

1.7 Objective

The objective of this dissertation is to create an optimal H_∞ control which ensures the maneuverability of a reentry lifting vehicle and its control throughout its reentry. The controller must guarantee that the vehicle reentering the atmosphere follows the trajectory desired, even when subjected to noise and disturbances during its flight.

Furthermore, it is desirable for the controller to be robust which implicates the capability of stabilizing the vehicle regardless of the number of disturbances applied and their magnitude.

The objective will be considered full-filled if the difference between a non-controlled and controller trajectory can be clearly observed and of course, if it shows the positive implication of having the controller applied to the presented dynamic system.

The final objective of this dissertation will reside in the insights on the efficiency of the H_∞ controller and the reasons behind it: not only the effectiveness of the controller must be studied, but also if it answers quickly to disturbances, and on which systems could it do an even more outstanding job.

1.8 Structure

The contents of this dissertation will begin with the Reentry Flight Dynamics Model (Chapter 2) where the dynamics and restrictions that make part of Reentry Trajectories will be explained. Following, the dissertation will move to the trajectory analysis (Chapter 3) where a trajectory that was already developed will be analyzed in order to check its validity and to verify if it can be useful or not in this H_∞.

Following the trajectory verification and validation, the project for the controller takes place (Chapter 4), being in this chapter where the controller and its methodology are fully explained. Finally, the controller will be subjected to disturbances and noise, allowing the representation of the results of its application (Chapter 5). The conclusions of the work done in the dissertation as well as possible next projects to be made on this matter will be suggested in Chapter 6.

Chapter 2

Reentry Flight Dynamics Model

To be capable of designing and projecting the controller for the RLV the need to use an estimation of trajectory surged. In this chapter, the equations that will allow the calculation of each variable that describes the movement of the RLV during its descent will be reviewed.

Additionally, the state vector on which the variables that describe the position and velocity of the RLV, as well as the control vector of its movement, will be presented. Through them, the full calculation of the reentry trajectory is achievable given the possibility to accompany the RLV in each step of its descent.

Finally, given that the reentry trajectory calculation is a highly non-linear problem that counts and obeys the constraints already explained, the equations used to calculate each one - Heating Rate, Dynamic Pressure and Maximum Deceleration - will be described.

2.1 Coordinate Frame

The coordinate system used for this dissertation will be a Planet-Fixed frame. Firstly, it is designed a Geocentric-Equatorial Coordinate Frame where its origin resides in the center of motion (COM) of the planet Earth. Its axis X will be directed to the Greenwich Meridian and the axis Y will be directed such that it lies in the equatorial plane and makes a 3-axis system with the axis X and Z with a $90°$ angle between each one [4, 10, 22]. The coordinate system can be seen in fig. (2.1):

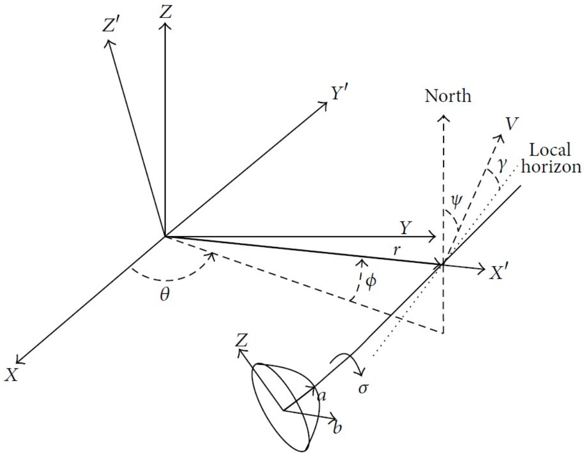

Figure 2.1: Coordinate Frame. [22]

where r represents the distance between the COM of the planet and the COM of the reentering vehicle. The longitude will then be represented by θ and the latitude by ϕ.

The symbol σ represents the angle between the vehicle longitudinal symmetry plane and the vertical plane, otherwise known as the bank angle and γ represents the velocity flight angle.

The letter V represents the velocity vector of the vehicle at a given moment in time and ψ is the heading angle measured from North.

Throughout this work, h will sometimes be used instead of r, while the only difference between these two variables is the Earth's radius:

$$r = h + R \tag{2.1}$$

with R representing the Earth's Medium Radius ($6.371.009\ m$).

2.2 Reentry Dynamics

The 3DOF equations of a hypersonic vehicle reentering the atmosphere consider earth as a spherical and non-rotating body, and are shown as in [23]:

$$\dot{\boldsymbol{h}} = v\ sin(\gamma) \tag{2.2}$$

$$\dot{\boldsymbol{\phi}} = \frac{v\ cos(\gamma)\ cos(\psi)}{r} \tag{2.3}$$

$$\dot{\boldsymbol{\theta}} = \frac{v\ cos(\gamma)\ sin(\psi)}{r\ cos(\phi)} \tag{2.4}$$

$$\dot{\boldsymbol{v}} = \frac{-D}{m} - g\ sin(\gamma) \tag{2.5}$$

$$\dot{\boldsymbol{\gamma}} = \frac{L\ cos(\sigma)}{v\ m} - \frac{g}{v}\ cos(\gamma) + \frac{v}{r}\ cos(\gamma) \tag{2.6}$$

$$\dot{\boldsymbol{\psi}} = \frac{L\ sin(\sigma)}{m\ v\ cos(\gamma)} + \frac{v}{r}\ cos(\gamma)\ sin(\psi)\ tan(\phi) \tag{2.7}$$

where v stands for the velocity relative to Earth as a scalar. The other variables were already explained in the previous sub-section. Earths gravity acceleration is represented by the letter

g and it's calculated according to the RLV's altitude h:

$$g = g_0 \left(\frac{R}{R+h} \right)^2 \tag{2.8}$$

where g_0 is the gravity Acceleration at sea level (g_0 = $9,80665 \ m/s$), R represents Earth's medium radius as stated previously and R + h represents the sum between Earth's medium radius and the RLV's altitude, which can be presented as r (eq. (2.1)).

Since the vehicle is an RLV, it will be subjected to both aerodynamic forces of lift L and drag D which can be calculated as follows:

$$L = \frac{1}{2} \rho \, v^2 \, S \, C_L \, (\alpha, M_a, \sigma, \delta_e) \tag{2.9}$$

$$D = \frac{1}{2} \rho \, v^2 \, S \, C_D \, (\alpha, M_a, \sigma, \delta_e) \tag{2.10}$$

where S is the reference area of the RLV and m the reference of its mass. C_L and C_D being the lift and drag coefficient, respectively, and will be calculated according to the AOA - α -, bank angle σ, elevator angle δ_e and Mach number M_a=$\frac{v}{sound \ velocity}$. The atmospheric density ρ is calculated by:

$$\rho = \rho_0 \ exp \left(-\frac{h}{h_s} \right) \tag{2.11}$$

where ρ_0 is the atmospheric density at sea level, h is the current altitude of the vehicle when compared to the sea level and h_s is the scalar height coefficient [12].

The lift and drag coefficient can be calculated as in [24]:

$$C_L = C_{L0} + C_{L\alpha} \, \alpha + \frac{\bar{c}}{2V} \, \left(C_{L\dot{\alpha}} \, \dot{\alpha} + C_{Lq_p} \, q_p \right) + C_{L\delta e} \, \delta_e \tag{2.12}$$

$$C_D = C_{D0} + C_{D\alpha} \, \alpha + \frac{\bar{c}}{2V} \, \left(C_{D\dot{\alpha}} \, \dot{\alpha} + C_{Dq_p} \, q_p \right) + C_{D\delta e} \, \delta_e \tag{2.13}$$

where q_p represents the pitch rate and α the AOA. C_L and C_D are calculated by several parts:

- C_{L0} and C_{D0} are related to the RLV body;

- $C_{L\alpha}$ and $C_{D\alpha}$ are related to the current AOA;

- $C_{L\delta_e}$ and $C_{D\delta_e}$ are related to the elevator's deflection.

To calculate the pitch rate, we first need to clarify the reasoning behind it. Considering the letter λ as the pitch angle, the following assumption can be made:

$$\lambda = \alpha + \gamma \tag{2.14}$$

that is, the pitch angle is the sum of the AOA - α - and the flight path angle - γ - which can be visualized in fig. (2.2).

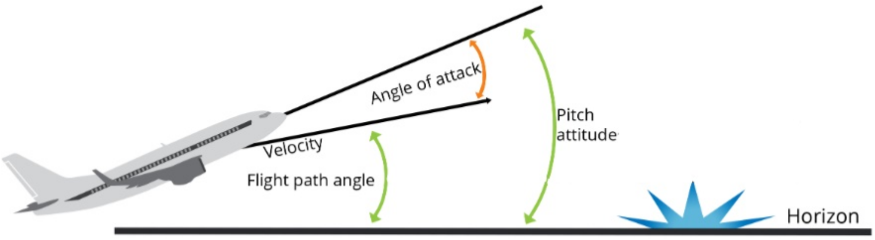

Figure 2.2: Representation of an Aircraft's Pitch Angle, adapted from [25].

With the value of the pitch angle λ, it is now possible to obtain the value of the pitch rate q by use of the following equation found in [24]:

$$\dot{\lambda} = q\ cos(\sigma) - h\ sin(\sigma) \tag{2.15}$$

Isolating q_p and deriving the eq. (2.14) it is now possible to calculate the pitch rate as:

$$q_p = \frac{h\ sin(\sigma) + \dot{\alpha} + \dot{\gamma}}{cos(\sigma)} \tag{2.16}$$

With the reentry dynamics fully explained it is now possible analyze its state vector to allow the control of RLV and monitor the aircraft along the reentry trajectory.

2.3 State Vector

To estimate the trajectory, the state vector of the RLV must describe its condition throughout all reentry phases. Based on the flight dynamics equations, the state vector of the vehicle can be described as:

$$x = \begin{bmatrix} \dot{h} \\ \dot{\phi} \\ \dot{\theta} \\ \dot{v} \\ \dot{\gamma} \\ \dot{\psi} \end{bmatrix} \tag{2.17}$$

where $[\dot{h}, \dot{\phi}, \dot{\theta}]$ represents the position variation vector in spherical coordinates and $[\dot{v}, \dot{\gamma}, \dot{\psi}]$ represents the velocity variation vector also in spherical coordinates:

- $\dot{h}$ – altitude variation of the RLV;
- $\dot{\phi}$ – latitude variation of the RLV;
- $\dot{\theta}$ – longitude variation of the RLV;
- $\dot{v}$ – velocity variation of the RLV;
- $\dot{\gamma}$ – flight variation path angle of the RLV;
- $\dot{\psi}$ – heading variation angle of the RLV.

With these variables in the state vector the projection of the controller and the constant monitoring of its flight throughout all phases of flight becomes possible.

2.4 Control Vector

The rotation of the vehicle or the variation of its AoA is controlled by the action of its aerodynamic surfaces, such as flaps, rudder, and elevator. Assuming β = 0 and $\dot{\beta}$ = 0 - which means the RLV drifting angle and its variation is zero - the control vector is represented as:

$$u = \begin{bmatrix} \dot{\alpha} \\ \dot{\sigma} \end{bmatrix} \tag{2.18}$$

With the state and control vector represented the system can now be described, being the constraints that will limit the flight profile of the RLV represented in the next subsection.

2.5 Applied Constraints

The constraints used to limit our problem were inspired by the work presented in [2, 3, 12, 26].

2.5.1 Heating Rate

$\dot{Q}_s$ is the heating rate of the vehicle at a certain point, which must be limited by the maximum heating rate the vehicle can endure and is calculated by:

$$\dot{Q}_s \cong k_Q \, v^3 \sqrt{\frac{\rho}{r_{nose}}} \leq \dot{Q}_{s_{max}} \tag{2.19}$$

where k_Q is the heating rate normalization constant, r_{nose} is the vehicle's nose radius and $\dot{Q}_{s_{max}}$ is the maximum heating rate the vehicle can withstand. The value $k_Q = 1,75E - 04\sqrt{kg/m}$ was used as in [3].

2.5.2 Dynamic Pressure

Dynamic pressure presents itself with the letter q and it is limited to control the hinge moment of an actuator in a determined range. The dynamic pressure must be less than a certain maximum value, and it is calculated by:

$$q = \frac{1}{2} \, \rho \, v^2 \leq q_{max} \tag{2.20}$$

2.5.3 Maximum Deceleration

As mentioned before, there will be a limit to how much deceleration will the vehicle be subjected to. In section (1.1) was stated that the maximum deceleration a human can withstand is 12 $g's$. However, it will be limited to 3 $g's$ not only for structural reasons but for the comfort and well-being of the RLV's crew.

The deceleration is calculated as:

$$a = \frac{v^2 \, \omega \, sin(\gamma)}{2e} \leq a_{max} \tag{2.21}$$

where ω represents the atmospheric scaled height, a parameter used to describe the density profile of the atmosphere. The letter e represents the base of the natural logarithm [2].

2.5.4 Controllability of the RLV

To ensure the controllability of the RLV we must ensure that the AoA, bank angle, elevator and rudder angle stay within certain limits:

$$\alpha_{min} \leq \alpha \leq \alpha_{max}, \ |\dot{\alpha}| \leq \dot{\alpha}_{max} \tag{2.22}$$

$$\sigma_{min} \leq \sigma \leq \sigma_{max}, \ |\dot{\sigma}| \leq \dot{\sigma}_{max} \tag{2.23}$$

being $\dot{\alpha}_{max}, \dot{\sigma}_{max} \leq 5°/s$, $\alpha_{min} = 0°$, $\alpha_{max} = 60°$, $\sigma_{min} = -89°$ and $\sigma_{max} = 90°$.

With the above-mentioned restrictions, we form our entry corridor (represented in fig. (1.5)) on which we will find the optimal trajectory for the RLV and then project the controller for it.

2.6 Output Vector

The output vector will be composed with the Geodetic Coordinates Variation - $\dot{\phi}$, $\dot{\theta}$ and $\dot{h}$ - making it possible to transform them into Geodesic coordinates if there is a desire to do so.

The output vector will then be as follows:

$$y = \begin{bmatrix} \dot{\phi} \\ \dot{\theta} \\ \dot{h} \end{bmatrix} \tag{2.24}$$

Chapter 3

Reentry Trajectory Analysis

This chapter will consist on the analysis of the trajectory on which the controller will be designed. To ensure the validity of the controller that will be developed, this trajectory must resemble one of a real shuttle - such as the *Orbiter*, for example - and follow the dynamics and restrictions explained throughout the previous chapters.

As the objective of this dissertation is not to develop a trajectory but to develop an optimal and robust controller that could be implemented on the RLV's software, the possibility to use an adequate trajectory already developed surged. Such trajectory was found and created by *Henrique Ferrolho* and its creation will be deeply explained in this chapter.

The code provided a trajectory of reentry that was inspired in the problem suggested in chapter 6 of "Practical Methods for Optimal Control and Estimation Using Nonlinear Programming" by *John T. Betts* [27].

3.1 Trajectory Estimation as an Optimal Control Problem

Designing the best possible reentry trajectory for a shuttle is a highly nonlinear estimation problem. The nonlinear behavior of this problem makes the use of a simple shooting method impossible.

John T. Betts presents a possible way to solve this problem, using the same reentry flight dynamics presented in chapter 2 of this dissertation (section 2.2). That is, all the equations that fully describe the RLV's state throughout its reentry are the same as in the problem presented. The restrictions used to solve the nonlinear problem revealed to be the same as in the previous chapter.

3.1.1 Objective Function

To reach the solution of the problem the need to set an objective function existed. There are three possibilities to consider in choosing the objective function behind the trajectory design algorithm. As shown in [27], the objective function can be the minimization of the heating rate of the RLV during reentry, the maximization of the cross-range of the vehicle during reentry or the maximization of the down-range of the vehicle during reentry. For the presented dissertation, the objective function will be the maximization of the cross-range of the RLV.

$$J = \phi(t_f) \tag{3.1}$$

in which J represents the objective function. Maximizing the cross-range of the vehicle is the same as maximizing the final latitude of the RLV, hence the transformation to ϕ in the previous formula.

The maximization of the down-range would produce the maximization of the longitude, which would also be a well-designed and possible desired trajectory, but the optimizer used for this project couldn't converge on a suitable solution for that objective function.

Initial and final conditions for the vehicle were also displayed. The initial conditions represent the beginning of the RLV's descent through Earth's Atmosphere as the final conditions represent the start of the TAEM, the phase on which the RLV's crew takes over the control and maneuverability of the vehicle. Both conditions were set in English Units, which will later be converted to SI units after the implemented code.

3.1.2 Initial conditions, RLV's characteristics and Final conditions

The initial conditions to the problem were first described in [27]. However, to further enhance the understanding of the problem, two problems were created differing only in the initial condition γ_i, both following the information found in [5]:

trajectory 1	**trajectory 2**
$h_i = 400.000\ ft$	$h_i = 400.000\ ft$
$\phi_i = 0\ deg$	$\phi_i = 0\ deg$
$\theta_i = 0\ deg$	$\theta_i = 0\ deg$
$v_i = 25.600\ ft/s$	$v_i = 25.600\ ft/s$
$\gamma_i = -1,1\ deg$	$\gamma_i = -5\ deg$
$\psi_i = 90\ deg$	$\psi_i = 90\ deg$

Table 3.1: Initial Conditions in Imperial Units

trajectory 1	**trajectory 2**
$h_i = 121.920\ m$	$h_i = 121.920\ m$
$\phi_i = 0\ rad$	$\phi_i = 0\ rad$
$\theta_i = 0\ rad$	$\theta_i = 0\ rad$
$v_i = 7.802,88\ m/s$	$v_i = 7.802,88\ m/s$
$\gamma_i = -0,0192\ rad$	$\gamma_i = -0,0873\ rad$
$\psi_i = 1,5708\ rad$	$\psi_i = 1,5708\ rad$

Table 3.2: Initial Conditions in SI units

with the following RLV characteristics and subjected to the following earth acceleration:

$$m = 203.000\ lb$$
$$S = 2.690\ ft^2$$
$$g_0 = 32,174\ ft/s^2$$

Table 3.3: RLV's Characteristics in Imperial Units

$$m = 92.079,251\ kg$$
$$S = 249,91\ m^2$$
$$g_0 = 9,8066\ m/s^2$$

Table 3.4: RLV's Characteristics in SI units

As mentioned before the reentry trajectory will end with the start of the TAEM phase which will start when the vehicle reaches the following numbers:

$$\begin{aligned} h_f &= 80.000\ ft \\ v_f &= 500\ ft/s \\ \gamma_f &= -5\ deg \end{aligned}$$

Table 3.5: Final Conditions in Imperial Units

$$\begin{aligned} h_f &= 24.384\ m \\ v_f &= 152,4\ m/s \\ \gamma_f &= -0,0873\ rad \end{aligned}$$

Table 3.6: Final Conditions in SI units

In this subsection, some alterations to the original setup were made because of the data given in [27] was not matching the information found in [5]. For example, the altitude of descent and the initial flight path angle (only of trajectory 1) - $400,000\ ft$ instead of the $260,000\ ft$, γ_i = -$1.1°$ instead of γ_i = -$1°$ - had to be changed. There were also some differences in the restriction values found in the code explained in the next section, which were corrected.

3.2 Algorithm of the Reference Reentry Trajectory

As mentioned before, since the objective of this dissertation is not to develop a reentry trajectory but an optimal and robust controller to be implemented in the RLV, the possibility of using an already existing code rose.

As a solution to this matter, a code that was part of an open MIT license was found. In this code, *Henrique Ferrolho* solved the exact problem of chapter 6 from [27] with the help of *JuMP*, a specific domain that belongs to *Julia*'s programming language. *Julia* presents itself as a language designed specifically for high performance. While the computing power needed is great, the achieved precision justifies the problem. Given the high difficulty of solving the reentry problem, *Henrique Ferrolho* decided to code in this language.

The *JuMP* domain is a modeling language that supports packages for mathematical optimization in *Julia*. It facilitates the formulation and solving of linear programming, integer programming, semidefinite programming, convex optimization, related classes of optimization problems, and constrained nonlinear optimization – which is the case of the problem presented [28].

The optimizer used to find the solution to the reentry trajectory problem was the interior-point optimizer. This optimizer is widely used in many different problems being capable of solving linear and nonlinear problems, according to the user's needs. The method uses the restrictions as guidelines and transforms them so that a linear program that can operate them. After doing so, Newton's method is applied to continuously obtain better solutions, until the optimal solution is found within the barriers formed by the restrictions of the problem [29].

Briefly explaining the code, the optimizer starts at the initial conditions described in subsection 3.1.2 and varies each parameter from the vehicle's state vector in a time step of 4 seconds, with the objective of maximizing the final cross range of the RLV's until the final conditions are reached. For each time step, an array for that specific time is being created such as:

$$x(t_k) = \begin{bmatrix} \dot{h}(t_k) \\ \dot{\phi}(t_k) \\ \dot{\theta}(t_k) \\ \dot{v}(t_k) \\ \dot{\gamma}(t_k) \\ \dot{\psi}(t_k) \end{bmatrix} \tag{3.2}$$

Using as control variables the following array:

$$u(t_k) = \begin{bmatrix} \dot{\alpha}(t_k) \\ \dot{\sigma}(t_k) \end{bmatrix} \tag{3.3}$$

where k represents the current cycle of the code. Compiling the arrays in a matrix will then allow the full study of the reentry trajectory of the vehicle and the projection of the code for the optimal controller.

In each step of the code the variables calculated were integrated resulting in the values of altitude, latitude, longitude, velocity, flight path angle, heading angle, angle of attack, and bank angle of the RLV:

$$\bar{x}(t_k) = \begin{bmatrix} h(t_k) \\ \phi(t_k) \\ \theta(t_k) \\ v(t_k) \\ \gamma(t_k) \\ \psi(t_k) \end{bmatrix} \tag{3.4}$$

$$\bar{u}(t_k) = \begin{bmatrix} \alpha(t_k) \\ \sigma(t_k) \end{bmatrix} \tag{3.5}$$

The code produced by *Henrique Ferrolho* can be found in [30] and is totally open for public use, being it as it is presented, or to change it in any way the user pleases. As stated before, the used code had some alterations when compared to the original one, since some of the constant values used in the original were not a match to a real shuttle as was explained in subsection 3.1.2.

3.3 Trajectory and Obtained Results

From this chapter on, the code used to design the controller will be made in *Python*. To do so, the matrix of variables that describes the trajectory was extracted from both cases (presented in table (3.1.2)). The matrix of variables that described the control variables of the vehicle was also extracted. Following, graphs were plotted to better see the trajectory mentioned.

The matrices extracted contained the final data, that is, the integrated data. This was a personal choice, justified by the following reasoning: if the data produced by *Julia* represented a trustworthy trajectory, I wanted to start with the raw data that is provided and recalculate every derivative or variation of all the variables inside the same program - *Python*. This way each error or imprecision was easily traceable and hopefully able to correct.

The generic matrix extracted for each case were as follows:

$$M = \begin{bmatrix} h_i & \dots & h_f \\ \phi_i & \dots & \phi_f \\ \theta_i & \dots & \theta_f \\ v_i & \dots & v_f \\ \gamma_i & \dots & \gamma_f \\ \psi_i & \dots & \psi_f \end{bmatrix} \tag{3.6}$$

in which the ”i” subscript represents the initial and the ”f” the final state of the system.

For the case with γ_i = -$1, 1°$, the matrix extracted will be named matrix T_j. For the other case in study, with γ_i = -$5°$, the matrix extracted will be named matrix Z_j. The ”j” subscript symbolizes the origin behind these matrices - Julia code. Each of the matrices has a dimension of 6 x 600, that is, 6 rows and 600 columns and can be described as:

$$T_j = M(\gamma_i = -1°) \qquad\qquad Z_j = M(\gamma_i = -5°) \tag{3.7}$$

To finalize the description of the movement of the RLV’s throughout its descend, further data must be retrieved from Julia code: the control matrix which describes the development of the angle of attack - α - and of the bank angle - σ:

$$N = \begin{bmatrix} \alpha_i & \dots & \alpha_f \\ \sigma_i & \dots & \sigma_f \end{bmatrix} \tag{3.8}$$

As previously, for the case with γ_i = -$1, 1^\circ$, the matrix extracted will be named matrix N_{T_j}. For the other case with γ_i = -5° the matrix extracted will be named matrix N_{Z_j}. The matrices can then be described as:

$$N_{T_j} = N(\gamma_i = -1^\circ) \qquad\qquad N_{Z_j} = N(\gamma_i = -5^\circ) \tag{3.9}$$

Finally, the time step t_s used to calculate each value of all variables extracted was $4\ seconds$ till it reached $2396\ seconds$, forming the vector:

$$t_s = \begin{bmatrix} 0 & 4 & \dots & 2392 & 2396 \end{bmatrix} \tag{3.10}$$

In the next subsection all the graphics obtained will be displayed, allowing the comparison of entering the atmosphere with a standard entry angle (γ_i = -$1, 1^\circ$) and with a deeper steep reentry (γ_i = -5°). Additionally, the restrictions displayed in eq. (2.19), (2.20) and in (2.21) will be described to see if any restriction surpasses its maximum allowed value.

3.3.1 First case, with γ_i = -$1, 1^\circ$

The results obtained by plotting the matrix T_j with the time step t_s were the following:

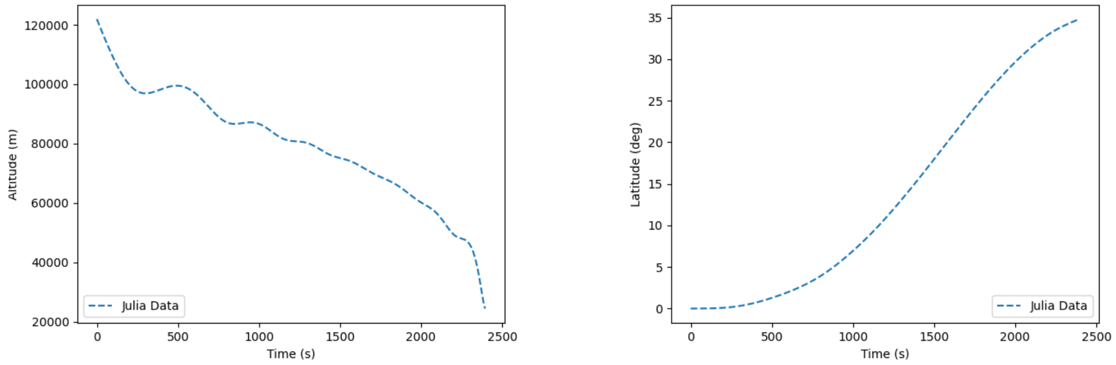

(a)

(b)

Figure 3.1: (a) RLV's altitude evolution for γ_i = -$1, 1^\circ$; (b) RLV's latitude evolution for γ_i = -$1, 1^\circ$

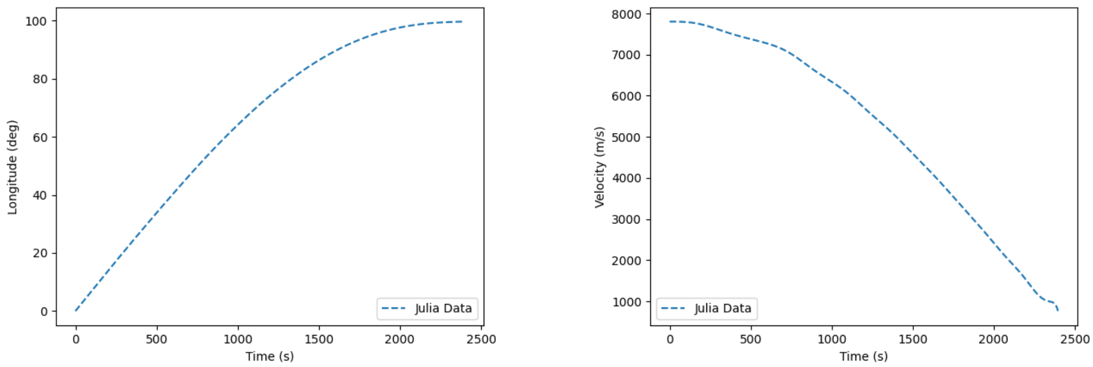

(a) (b)

Figure 3.2: (a) RLV's longitude evolution for γ_i = -1, 1°; (b) RLV's velocity evolution for γ_i = -1, 1°

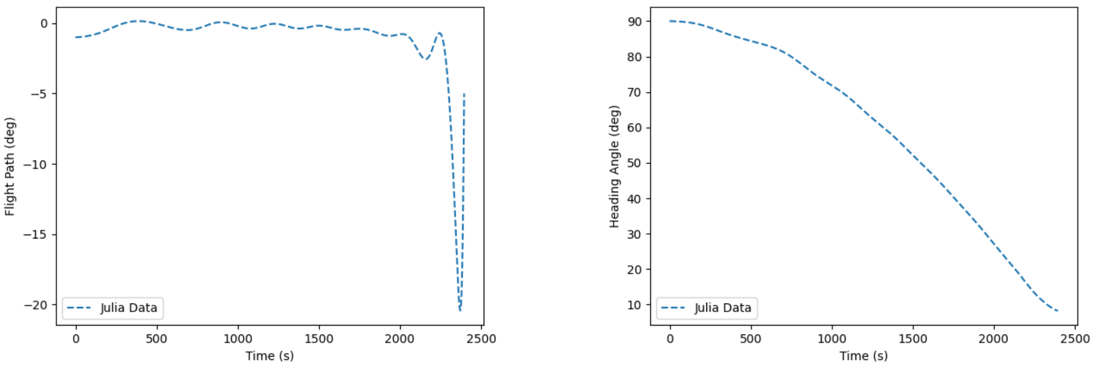

(a) (b)

Figure 3.3: (a) RLV's flight path angle evolution for γ_i = -1, 1°; (b) RLV's heading angle evolution for γ_i = -1, 1°

Secondly, the values obtained by plotting the Matrix N_{T_j} with the time step t_s:

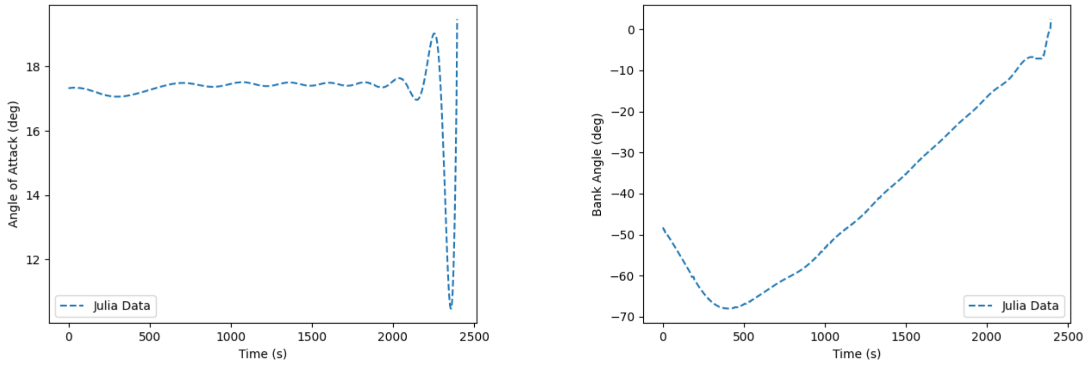

(a) (b)

Figure 3.4: (a) RLV's angle of attack evolution with for γ_i = -1, 1°; (b) RLV's bank angle evolution for γ_i = -1, 1°

The values of the restrictions were then calculated as explained in 2.5:

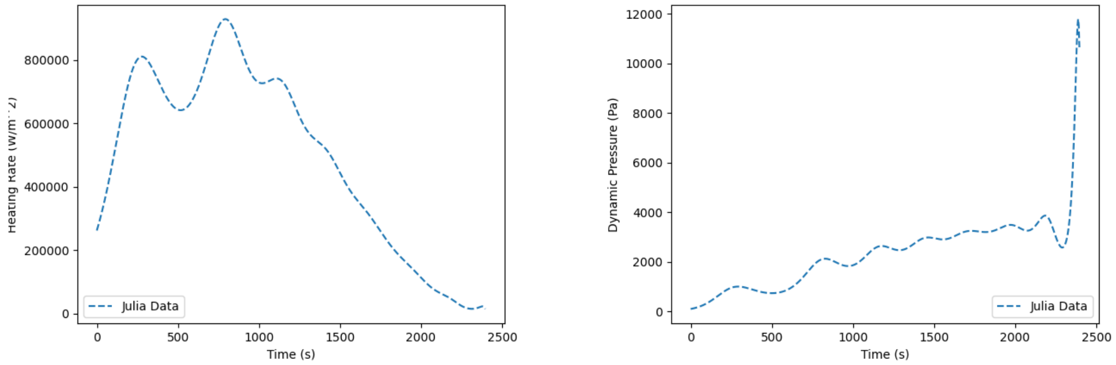

(a) (b)

Figure 3.5: (a) RLV's Heating Rate for γ_i = -1, 1°; (b) RLV's dynamic pressure for γ_i = -1, 1°

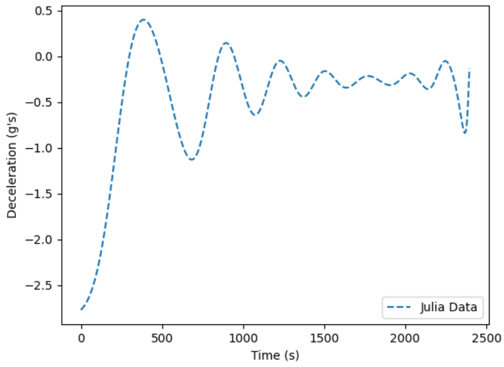

Figure 3.6: RLV's deceleration for γ_i = -1, 1°

The 3D space shuttle trajectory obtained for this case using the values of ϕ, θ and h:

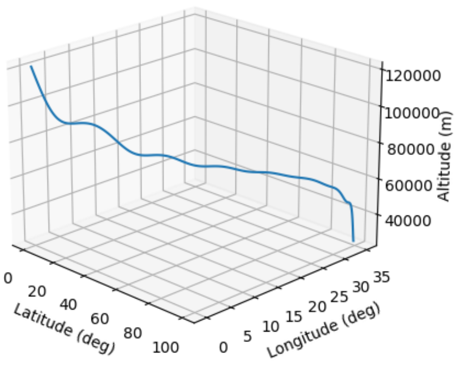

Figure 3.7: Space Shuttle Trajectory for γ_i = -1, 1°

3.3.2 Second case, with γ_i = -5°

The results obtained by plotting the matrix Z_j with the time step t_s were the following:

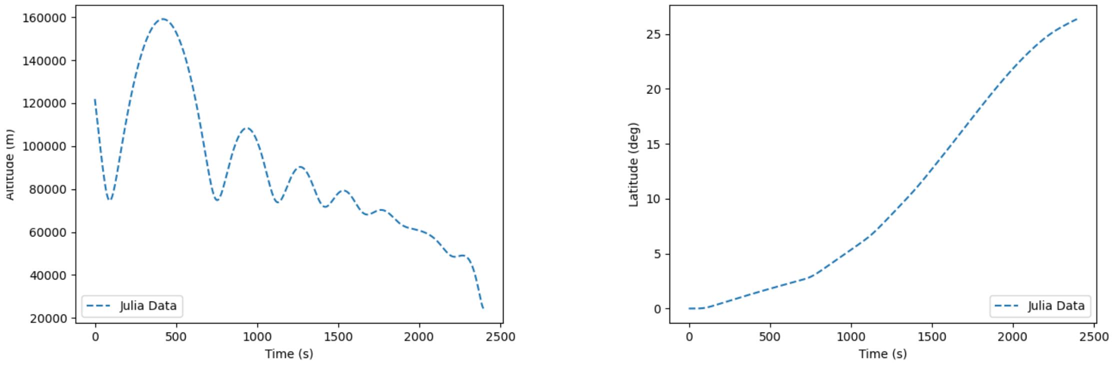

(a) (b)

Figure 3.8: (a) RLV's altitude evolution for γ_i = -5°; (b) RLV's latitude evolution for γ_i = -5°

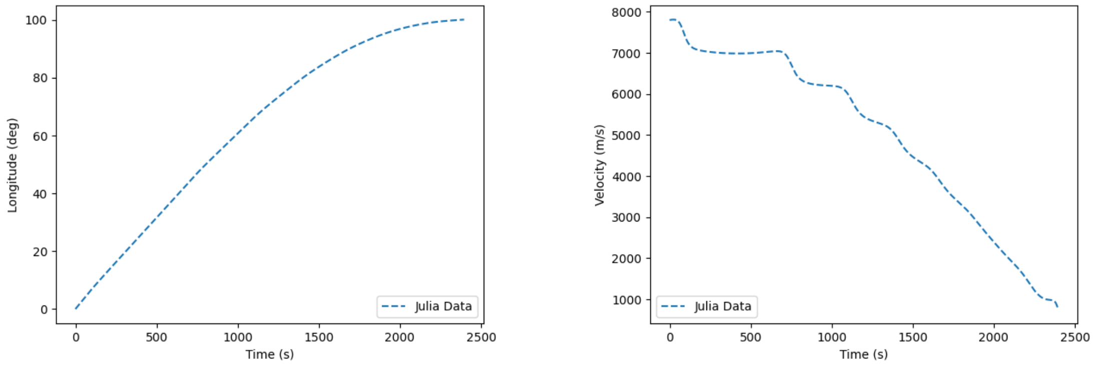

(a) (b)

Figure 3.9: (a) RLV's longitude evolution for γ_i = -5°; (b) RLV's velocity evolution for γ_i = -5°

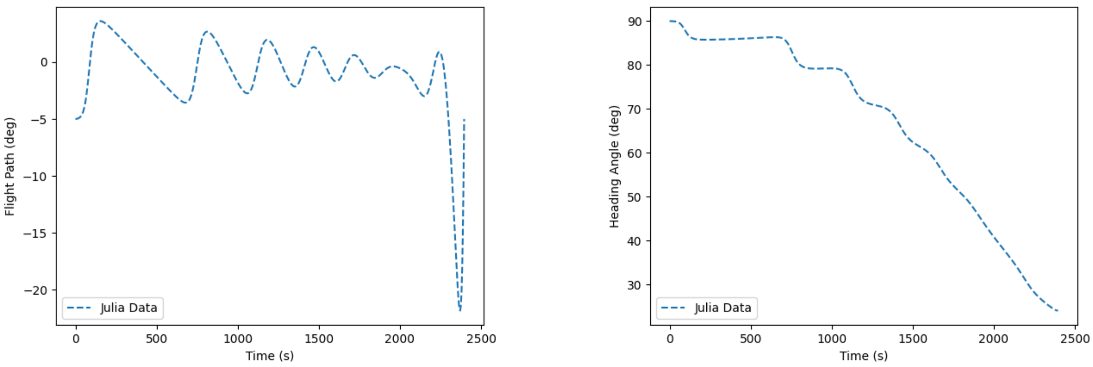

(a) (b)

Figure 3.10: (a) RLV's flight path angle evolution for γ_i = -5°; (b) RLV's heading angle evolution for γ_i = -5°

Secondly, the values obtained by plotting the Matrix N_{Z_j} with the time step t_s:

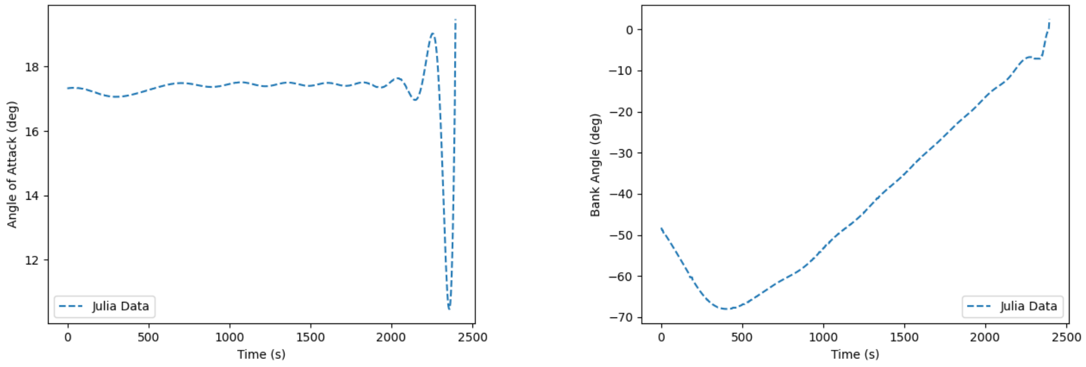

(a)

(b)

Figure 3.11: (a) RLV's angle of attack evolution for γ_i = -5°; (b) RLV's bank angle evolution for γ_i = -5°

The values obtained for the constraints explained in 2.5 were as follows:

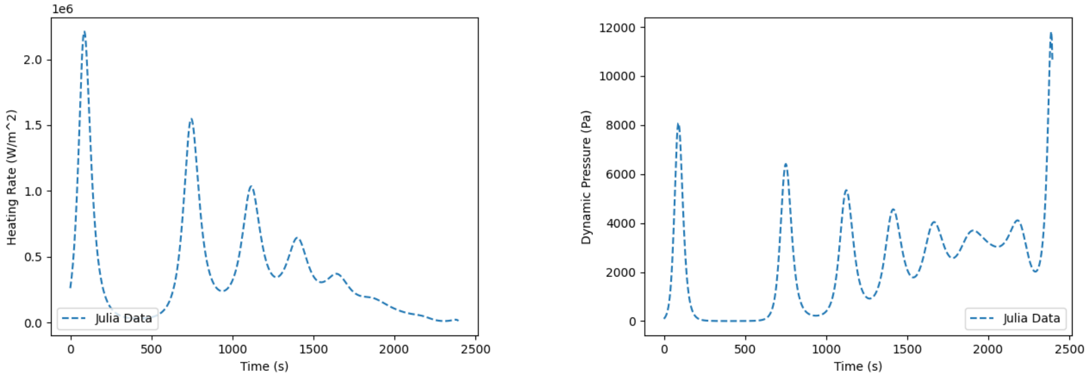

(a)

(b)

Figure 3.12: (a) RLV's Heating Rate for γ_i = -5°; (b) RLV's dynamic pressure for γ_i = -5°

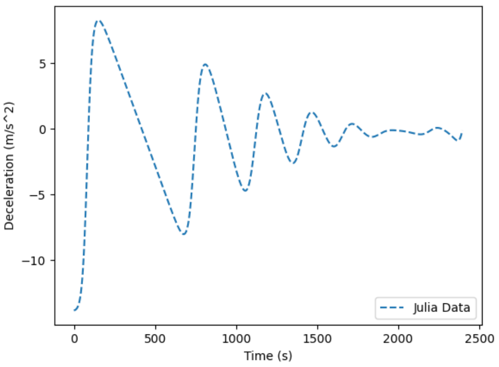

Figure 3.13: RLV's deceleration for γ_i = -5°

The 3D space shuttle trajectory obtained for this case using the values of ϕ, θ and h:

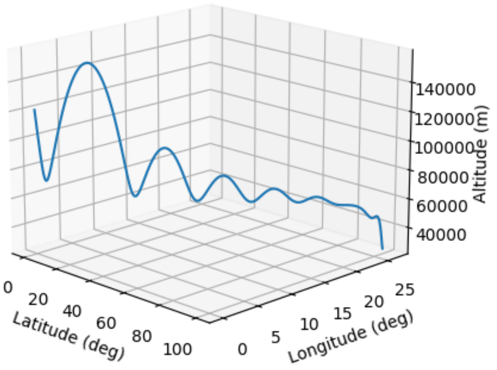

Figure 3.14: Space Shuttle Trajectory for γ_i = -5°

3.4 Discussion of Results

By observing the two cases shown - subsection 3.3.1 and subsection 3.3.2 - we can see that a reentry trajectory with a steeper flight path angle, produces severe changes in the constraints studied and therefore, in the reentry trajectory itself.

Firstly, through mere analysis of the difference between the graphics (3.5(a)) and (3.12(a)), we can see that the heating rate massively impacts the vehicle on the second case reaching values of $2.210.000$ W/m^2, while the values of the first case reach only up to 930.000 W/m^2. Being subjected to a less powerful heating flux presents a pleasing factor for all the tiles and materials on its TPS, especially for its maintenance and integrity.

There is also a significant difference between the two cases on the deceleration of the RLV. In the second case, the deceleration of the RLV reaches values of -13 g's which is more than a human can withstand. A steeper reentry needs to decelerate much faster than one with a smaller flight path angle of reentry making it impossible for the RLV to be occupied by human life - which is, in the case of a shuttle, an impossible trajectory.

It is also possible to observe differences in the dynamic pressure felt by the RLV in both cases. However, it is not such a significant difference when compared to the other two restrictions where we can clearly see the consequences of a steeper reentry trajectory.

On all the graphics displayed, it can be verified that not only the maximum values of the restrictions were in the second case violated, but the variations of each restriction and variable were remarkable, being surely felt inside the RLV and potentially setting its structure, integrity and mission at risk.

In this dissertation the trajectory followed will be the first example. Entering with a flight path angle γ_i = -$1, 1^{\circ}$ is indeed closer to a standard shuttle reentry trajectory, as it represents a trajectory on which the deceleration of the RLV is bearable, its heating rate does not exceed the maximum heating rate of a shuttle and its dynamic pressure is more balanced.

Chapter 4

Design of the Optimal Controller

In this chapter, the development of the robust controller for the reentry motion of the RLV will be described. Each thought taken to do so will also be explained in this chapter.

To start the development of the algorithm behind the controller, it is firstly needed to obtain functions that best describe the data obtained and graphically displayed in figs.(3.1), (3.2), (3.3) and (3.4). That is, to estimate functions that describe the altitude, latitude, longitude, velocity, flight path angle, heading angle, angle of attack, and bank angle of the RLV throughout time.

Secondly, given that the reentry problem is a highly non-linear one, the need to proceed to its linearization appears, to allow the afterward calculations and H_∞ methodology. The need to proceed to this linearization will be briefly described in this chapter.

With the system fully linearized, the state feedback controller H_∞ concept shall be introduced and it will be revealed why it was thought to be the correct type of optimal controller to use in this case.

Finally, the architectural procedure behind the algorithm of the controller itself will be summarized. Alterations made on the standard method were made and will be described.

4.1 Functions Extracted

After obtaining the graphs presented in figs. (3.1), (3.2), (3.3) and (3.4) functions that estimate the development of these variables needed to be acquired.

Python offered a solution: a tool named *Curve Fit*, by the library *Scypy*, in which it automatically calculates the best approximate functions existing between the independent variables - h, ϕ, θ, v, γ, ψ, α and σ - and their dependent one - t - using non-linear least-squares method. To give a more perceptible example, the estimate functions retrieved for each of these variables were the following:

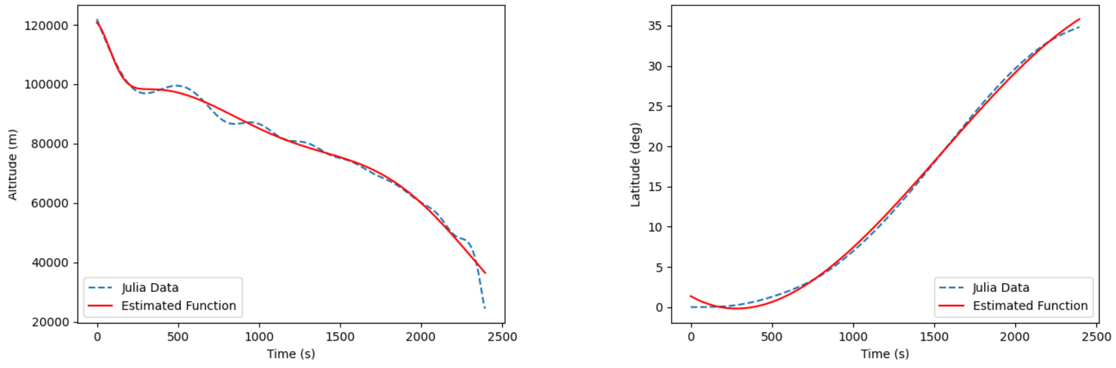

(a) (b)

Figure 4.1: (a) RLV's Altitude Estimated Function; (b) RLV's Latitude Estimated Function

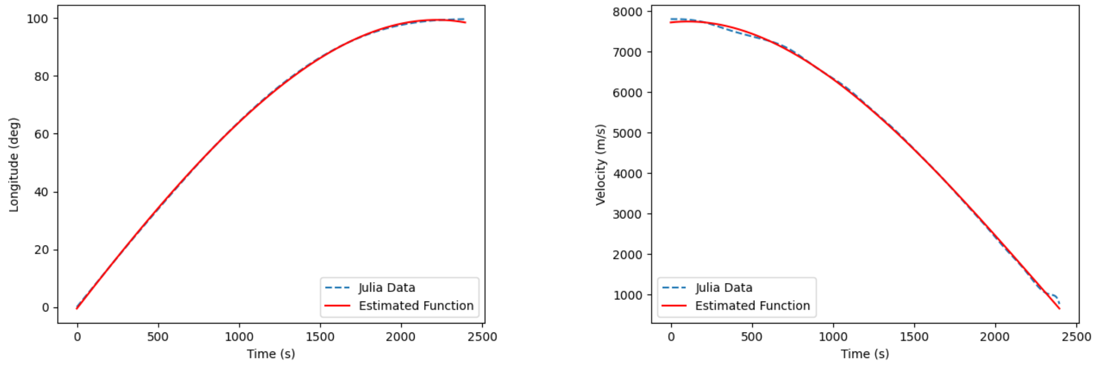

(a) (b)

Figure 4.2: (a) RLV's Longitude Estimated Function; (b) RLV's Velocity Estimated Function

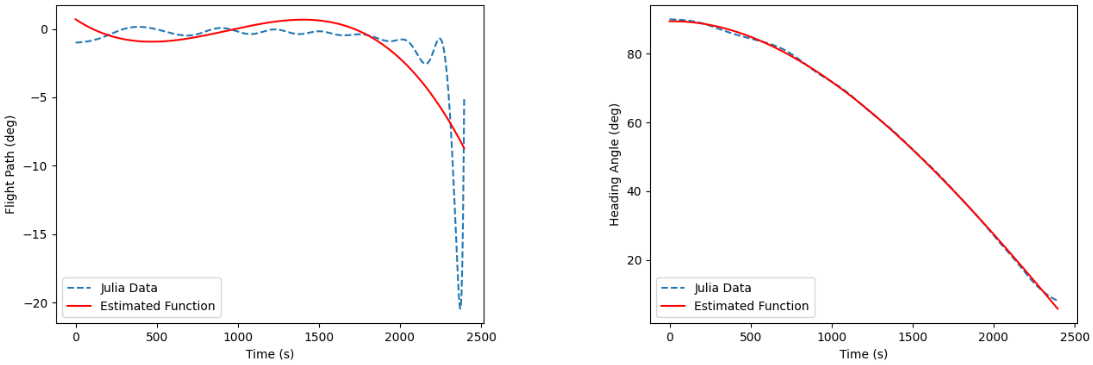

(a) (b)

Figure 4.3: (a) RLV's Flight Path Angle Estimated Function; (b) RLV's Heading Angle Estimated Function

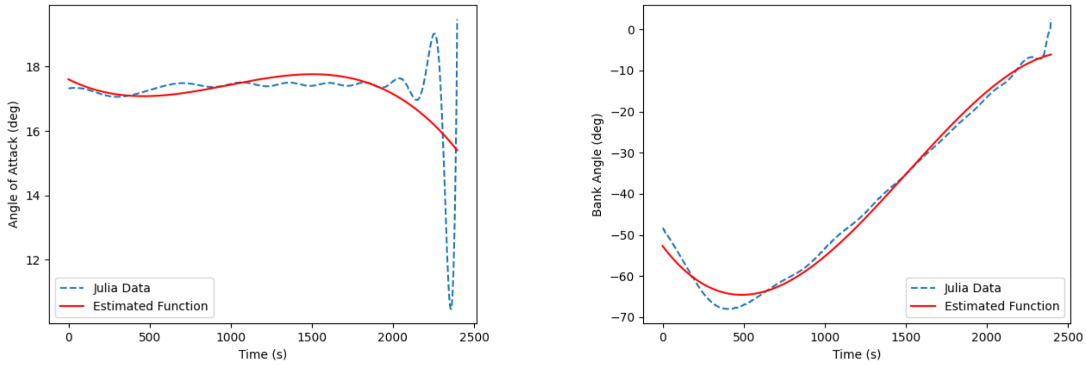

(a) (b)

Figure 4.4: (a) RLV's Angle of Attack Estimated Function; (b) RLV's Bank Angle Estimated Function

As stated previously, the final variations of the flight path angle and angle of attack come from within the *Julia* code on which its optimizer produced that abnormal variation. The procedure made to partly compensate this was to estimate both functions until the variation began, which meant to estimate the functions until $t \approx 2200 seconds$.

It is important to state that *Curve Fit* itself wasn't able to reproduce good estimate functions using *Fourier*, *High Gaussian*, *Exponential* or *Power Modules* for the development of the variables presented, making it harder to reproduce well-estimated data. The main functions *Curve Fit* used with finesse to estimate the data desired were *Polynomial* functions or *Gaussian* but with 2-3 maximum terms.

With all these factors in mind, it is reasonable to affirm that the estimated data represents satisfying results of function estimation for all variables, making it possible to obtain the following functions:

$$\dot{\boldsymbol{h}} = 96939.949\, e^{-\frac{t-74.941}{308.902}} + 46501.781\, e^{-\frac{t-468.650}{204.130}} + 30702.078\, e^{-\frac{t+8.821}{38.193}} \tag{4.1}$$

$$\dot{\boldsymbol{\phi}} = -3.038E-07\, t^3 + 3.5360E-04\, t^2 - 4.531E-02\, t + 1.363E+00 \tag{4.2}$$

$$\dot{\boldsymbol{\theta}} = -2.291E-07\, t^3 - 7.055E-05\, t^2 + 2.890E-01\, t - 5.414E-01 \tag{4.3}$$

$$\dot{\boldsymbol{v}} = 1.955E-05\, t^3 - 3.438E-02\, t^2 + 1.775E+00\, t + 7.721E+03 \tag{4.4}$$

$$\dot{\boldsymbol{\gamma}} = -2.542E-07\, t^3 + 1.784E-04\, t^2 - 3.136E-02\, t + 7.021E-01 \tag{4.5}$$

$$\dot{\boldsymbol{\psi}} = 1.578E-07\, t^3 - 3.328E-04\, t^2 + 3.070E-03\, t + 8.944E+01 \tag{4.6}$$

$$\dot{\boldsymbol{\alpha}} = -7.735E-08\, t^3 + 5.704E-05\, t^2 - 1.009E-02\, t + 1.760E+01 \tag{4.7}$$

$$\dot{\boldsymbol{\sigma}} = -8.991E-07\, t^3 + 1.015E-03\, t^2 - 2.077E-01\, t + -5.271E+01 \tag{4.8}$$

With these equations fully calculated is now possible to estimate the state and control of the vehicle in each time step.

4.2 Linearization of the system

Despite the fact that this system is a highly-nonlinear one, it is possible to approximate it to a rather linear behavior within a certain operating range of an equilibrium point, as stated in [31]. The calculation of equilibrium points is made by fixing a given $u = u^*$ and calculating the respective equilibrium state $x = x^*$ - which becomes the equilibrium point.

Solving the highly-nonlinear system as it was would be unfeasible, whereas solving the approximate system of linear differential equations is achievable. The application and configuration of the H_∞ controller is now within reach, where it wouldn't be without the linearization of the initial system.

On the other hand, using this method may produce some inaccuracies on the neighborhood of the equilibrium points, given that the result from the nonlinear system is only exactly the same as in the linear system at those specific points. Nevertheless, the advantages of using the linearization procedure deeply compensate for the consequential disadvantages [32].

After linearization, the system can be described as:

$$\Sigma = \begin{cases} \dot{x}(t) = A(t)x(t) + B(t)u(t) \\ y(t) = Ex(t) \end{cases} \tag{4.9}$$

where A is the state matrix, B the control matrix and E the output matrix.

Considering $x(t)$ as previous described in eq. (3.2), the state of the system can also be referred as:

$$f_1(x,u) = \dot{h} \tag{4.10}$$

$$f_2(x,u) = \dot{\phi} \tag{4.11}$$

$$f_3(x,u) = \dot{\theta} \tag{4.12}$$

$$f_4(x,u) = \dot{v} \tag{4.13}$$

$$f_5(x,u) = \dot{\gamma} \tag{4.14}$$

$$f_6(x,u) = \dot{\psi} \tag{4.15}$$

where each function f_n is related to the state x and the control vector u at a given moment in time. The matrix f can then be defined as:

$$f(x,u) = \begin{bmatrix} f_1(h,\phi,\theta,v,\gamma,\psi,\alpha,\sigma) \\ f_2(h,\phi,\theta,v,\gamma,\psi,\alpha,\sigma) \\ f_3(h,\phi,\theta,v,\gamma,\psi,\alpha,\sigma) \\ f_4(h,\phi,\theta,v,\gamma,\psi,\alpha,\sigma) \\ f_5(h,\phi,\theta,v,\gamma,\psi,\alpha,\sigma) \\ f_6(h,\phi,\theta,v,\gamma,\psi,\alpha,\sigma) \end{bmatrix} \tag{4.16}$$

The linearization starts by obtaining the matrices A and B described in eq. (4.9). To do so, each function f_n must be derived for each variable as is shown in section 2 of [31]. The matrix A is then described as:

$$A = \begin{bmatrix} \frac{\partial(f_1)}{\partial(h)}(h^*,\phi^*,\theta^*,v^*,\gamma^*,\psi^*,\alpha^*,\sigma^*) & \dots & \frac{\partial(f_1)}{\partial(\psi)}(h^*,\phi^*,\theta^*,v^*,\gamma^*,\psi^*,\alpha^*,\sigma^*) \\ \frac{\partial(f_2)}{\partial(h)}(h^*,\phi^*,\theta^*,v^*,\gamma^*,\psi^*,\alpha^*,\sigma^*) & \dots & \frac{\partial(f_2)}{\partial(\psi)}(h^*,\phi^*,\theta^*,v^*,\gamma^*,\psi^*,\alpha^*,\sigma^*) \\ \frac{\partial(f_3)}{\partial(h)}(h^*,\phi^*,\theta^*,v^*,\gamma^*,\psi^*,\alpha^*,\sigma^*) & \dots & \frac{\partial(f_3)}{\partial(\psi)}(h^*,\phi^*,\theta^*,v^*,\gamma^*,\psi^*,\alpha^*,\sigma^*) \\ \frac{\partial(f_4)}{\partial(h)}(h^*,\phi^*,\theta^*,v^*,\gamma^*,\psi^*,\alpha^*,\sigma^*) & \dots & \frac{\partial(f_4)}{\partial(\psi)}(h^*,\phi^*,\theta^*,v^*,\gamma^*,\psi^*,\alpha^*,\sigma^*) \\ \frac{\partial(f_5)}{\partial(h)}(h^*,\phi^*,\theta^*,v^*,\gamma^*,\psi^*,\alpha^*,\sigma^*) & \dots & \frac{\partial(f_5)}{\partial(\psi)}(h^*,\phi^*,\theta^*,v^*,\gamma^*,\psi^*,\alpha^*,\sigma^*) \\ \frac{\partial(f_6)}{\partial(h)}(h^*,\phi^*,\theta^*,v^*,\gamma^*,\psi^*,\alpha^*,\sigma^*) & \dots & \frac{\partial(f_6)}{\partial(\psi)}(h^*,\phi^*,\theta^*,v^*,\gamma^*,\psi^*,\alpha^*,\sigma^*) \end{bmatrix} \tag{4.17}$$

where each element of the matrix is calculated according to the equilibrium state x^* corresponding to the equilibrium point u^*, that is, by using the functions extracted in subsection

4.1 in each time step. The matrix B will then be defined as:

$$B = \begin{bmatrix} \frac{\partial(f_1)}{\partial(\alpha)}(h^*, \phi^*, \theta^*, v^*, \gamma^*, \psi^*, \alpha^*, \sigma^*) & \frac{\partial(f_1)}{\partial(\sigma)}(h^*, \phi^*, \theta^*, v^*, \gamma^*, \psi^*, \alpha^*, \sigma^*) \\ \frac{\partial(f_2)}{\partial(\alpha)}(h^*, \phi^*, \theta^*, v^*, \gamma^*, \psi^*, \alpha^*, \sigma^*) & \frac{\partial(f_2)}{\partial(\sigma)}(h^*, \phi^*, \theta^*, v^*, \gamma^*, \psi^*, \alpha^*, \sigma^*) \\ \frac{\partial(f_3)}{\partial(\alpha)}(h^*, \phi^*, \theta^*, v^*, \gamma^*, \psi^*, \alpha^*, \sigma^*) & \frac{\partial(f_3)}{\partial(\sigma)}(h^*, \phi^*, \theta^*, v^*, \gamma^*, \psi^*, \alpha^*, \sigma^*) \\ \frac{\partial(f_4)}{\partial(\alpha)}(h^*, \phi^*, \theta^*, v^*, \gamma^*, \psi^*, \alpha^*, \sigma^*) & \frac{\partial(f_4)}{\partial(\sigma)}(h^*, \phi^*, \theta^*, v^*, \gamma^*, \psi^*, \alpha^*, \sigma^*) \\ \frac{\partial(f_5)}{\partial(\alpha)}(h^*, \phi^*, \theta^*, v^*, \gamma^*, \psi^*, \alpha^*, \sigma^*) & \frac{\partial(f_5)}{\partial(\sigma)}(h^*, \phi^*, \theta^*, v^*, \gamma^*, \psi^*, \alpha^*, \sigma^*) \\ \frac{\partial(f_6)}{\partial(\alpha)}(h^*, \phi^*, \theta^*, v^*, \gamma^*, \psi^*, \alpha^*, \sigma^*) & \frac{\partial(f_6)}{\partial(\sigma)}(h^*, \phi^*, \theta^*, v^*, \gamma^*, \psi^*, \alpha^*, \sigma^*) \end{bmatrix} \tag{4.18}$$

whereas in the previous case of matrix A, the elements of the matrix are calculated according to the equilibrium state x^* corresponding to the equilibrium point u^*.

Finally, with the linearization of the system completed, it is now possible to obtain the values of each variable at any moment in time. This allows for the implementation of the controller algorithm given the fact that it allows for the study of its actuation and performance.

4.3 H_∞ Optimal Control with State-Feedback

A State-Feedback system is a controllable system on which the eigenvalues of the matrix A are used to calculate the feedback gain matrix K which is then used to calculate the new control that is set into the system's plant [33]. Essentially, it's a system that can react to a certain disturbance through the calculation of K and then use it to calculate the new control vector u, giving ”feedback” to the system.

The H_∞ methods are considered in control theory a fine solution to create controllers in which stabilization of the system is achieved with great performance. It has had a great impact on the development of control systems throughout the decades of 1980 and 1990 [34]

This method is then used for cases when the objective is to achieve a robust and optimal controller, as it happens in this dissertation. As stated in [34]: *”H_∞ techniques have the advantage over classical control techniques in which the techniques are readily applicable to problems involving multi-variable systems with cross-coupling between channels; disadvantages of H_∞ techniques include the high level of mathematical understanding needed to apply them successfully and the need for a reasonably good model of the system to be controlled.”*

The functioning of the H_∞ controller can be theoretically visualized in [35]:

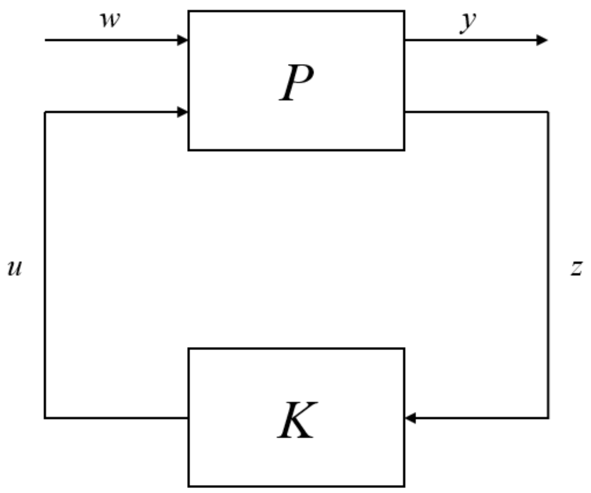

Figure 4.5: H_∞ Method Block Diagram. [35]

where P represents the plant of the system proposed, the z the alteration of the plant provoked by the external disturbance w, K represents the controller designed, u the effective control presented to the plant to begin the stabilization of the RLV and y which represents the final output of the system.

To calculate the plant P, the reasoning showed in [36] was followed: given the disturbance attenuation $\mu > 0$ the system Σ is considered *stabilizable* with the constant μ if there exists a controller capable of internally stabilizing it in the closed-loop system.

Furthermore, being the positive definite matrices Q, R, ζ and E - State Weighting Matrix, Control Weighting Matrix, Disturbance Matrix and Output Matrix, respectively - described as:

$$Q = Q_{intensity} * \begin{bmatrix} 1 & 0 & 0 & 0 & 0 & 0 \\ 0 & 1 & 0 & 0 & 0 & 0 \\ 0 & 0 & 1 & 0 & 0 & 0 \\ 0 & 0 & 0 & 1 & 0 & 0 \\ 0 & 0 & 0 & 0 & 1 & 0 \\ 0 & 0 & 0 & 0 & 0 & 1 \end{bmatrix} \tag{4.19}$$

$$R = 0.8 * \begin{bmatrix} 1 & 0 \\ 0 & 1 \end{bmatrix} \tag{4.20}$$

$$\zeta = \begin{bmatrix} 1 & 0 & 0 & 0 & 0 & 0 \\ 0 & 1 & 0 & 0 & 0 & 0 \\ 0 & 0 & 1 & 0 & 0 & 0 \\ 0 & 0 & 0 & 1 & 0 & 0 \\ 0 & 0 & 0 & 0 & 1 & 0 \\ 0 & 0 & 0 & 0 & 0 & 1 \end{bmatrix} \tag{4.21}$$

$$E = \begin{bmatrix} 0 & 1 & 0 & 0 & 0 & 0 \\ 0 & 0 & 1 & 0 & 0 & 0 \\ 1 & 0 & 0 & 0 & 0 & 0 \end{bmatrix} \tag{4.22}$$

and using the Algebraic Ricatti Equation - ARE:

$$PA + A'P - \frac{1}{\varepsilon}PBR^{-1}B'P + \frac{1}{\mu}P\zeta\zeta'P + \frac{1}{\mu}E'E + \varepsilon Q = 0 \tag{4.23}$$

with $\mu > 0$, the positive-definite solution P can be found as long as there exists a solution to this ARE in which $\varepsilon > 0$. In this case:

$$\mu = 100 \quad \varepsilon = 0.5 \tag{4.24}$$

If such conditions are satisfied, it is now possible to affirm that the system Σ is *stabilizable* with the disturbance attenuation μ [36]. Then, the controller matrix K described in fig. (4.5) can be calculated as:

$$K = \frac{-R^{-1}B'P}{2\varepsilon} \tag{4.25}$$

The $Q_{intensity}$ represents the fact that the matrix Q was, in this dissertation, variable throughout time. This fact will be addressed and justified later, but generally, Q has a fixed value in control algorithms.

In a more succinct way, in this dissertation the plant P represents the full dynamic system Σ. The H_∞ controller will be capable of finding the matrix K that can minimize the impact of the disturbance w on the output y under the constraint that the feedback gain matrix K can stabilize the plant P [37].

4.3.1 H_∞ ARE simplification

As it has been proven, the resolution complexity of the ARE shown before is quite considerable. Consequently, there were some alterations applied to the method explained previously in order to facilitate the use of the *Python* software and already existing functions within its programs. To do so the procedure was the following, step-by-step:

1. Creation of a transfer matrix F, with $\mu > 0$ such that all its eigenvalues were positive:

$$F = \frac{1}{\varepsilon}BR^{-1}B' - \frac{1}{\mu}\zeta\zeta' \tag{4.26}$$

2. Create a matrix $\bar{Q}$, a variation of the matrix Q:

$$\bar{Q} = \frac{1}{\mu}E'E + \varepsilon Q \tag{4.27}$$

3. Calculate the square root matrix of F represented by G:

$$G = sqrtm(F) \tag{4.28}$$

4. Finally, the use of a normal LQR function can be used such that:

$$[K_{no\,use}, P, V] = lqr(A, G, \bar{Q}, I_6) \tag{4.29}$$

As seen in eq. (4.25), the controller is calculated with the usage of the matrices R, B, P and the scalar value ε. The $K_{no\,use}$ calculated with the usage of the before-mentioned simplification is not correct, due to the fact that it is calculated assuming the LQR method and the inputs shown $(A, G, \bar{Q}, I_d)$ which is:

$$K = I_d^{-1}\, G'\, P \tag{4.30}$$

which would never give the same results as in eq. (4.25). However, through the simplification procedure shown, the matrix P is well calculated so it can be used along with the matrix R and B to calculate the real controller matrix K, which is what was implemented.

The next and final step of the calculation of the controller is to use the matrix K obtained previously and calculate the control that will be injected in the plant of the system in order to correct the path of the RLV. The control vector u is calculated as:

$$u(t) = -K\, x(t) \tag{4.31}$$

4.4 Recalculation of 3DOF equations

An alteration to the regular H_∞ has been proposed and applied: the matrix B, in each time step, nulls the possible alterations made to the RLV's altitude, latitude and longitude - $\dot{h}$, $\dot{\phi}$ and $\dot{\theta}$, respectively - given the fact that none of the equations used to calculate each of these variables depends on α or of σ. In a more illustrative way, what is being affirmed is that:

$$\frac{\partial(\dot{h})}{\partial(\alpha)}, \frac{\partial(\dot{h})}{\partial(\sigma)}, \frac{\partial(\dot{\phi})}{\partial(\alpha)}, \frac{\partial(\dot{\phi})}{\partial(\sigma)}, \frac{\partial(\dot{\theta})}{\partial(\alpha)}, \frac{\partial(\dot{\theta})}{\partial(\sigma)} = 0 \tag{4.32}$$

Consequently, the solution found was to calculate the differences set up to all the remaining variables and re-calculate all system variables using the equations described back in section 2.2.

More accurately describing, what was made was the following:

1. Calculation of $\dot{x}(t)$ which produces the values of $\ddot{h}(t)$, $\ddot{\phi}(t)$, $\ddot{\theta}(t)$, $\ddot{v}(t)$, $\ddot{\gamma}(t)$, $\ddot{\psi}(t)$ using the linearized system of eq. (4.9);

2. Using trapezoidal and Euler integration method [38], calculate the new values of h, ϕ, θ, v, γ and ψ:

$$h(t) = \frac{\ddot{h}(t) + \ddot{h}(t-s)}{2}\, ts^2 + \dot{h}(t-ts)\, ts + h^*(t) \tag{4.33}$$

$$\phi(t) = \frac{\ddot{\phi}(t) + \ddot{\phi}(t-s)}{2}\, ts^2 + \dot{\phi}(t-ts)\, ts + \phi^*(t) \tag{4.34}$$

$$\theta(t) = \frac{\ddot{\theta}(t) + \ddot{\theta}(t-s)}{2}\, ts^2 + \dot{\theta}(t-ts)\, ts + \theta^*(t) \tag{4.35}$$

$$v(t) = \frac{\ddot{v}(t) + \ddot{v}(t-s)}{2}\, ts^2 + \dot{v}(t-ts)\, ts + v^*(t) \tag{4.36}$$

$$\gamma(t) = \frac{\ddot{\gamma}(t) + \ddot{\gamma}(t-s)}{2}\, ts^2 + \dot{\gamma}(t-ts)\, ts + \gamma^*(t) \tag{4.37}$$

$$\psi(t) = \frac{\ddot{\psi}(t) + \ddot{\psi}(t-s)}{2}\, ts^2 + \dot{\psi}(t-ts)\, ts + \psi^*(t) \tag{4.38}$$

3. Using the Euler method on the control variables α and σ:

$$\alpha(t) = \dot{\alpha}(t-ts)\, ts + \alpha^*(t) \tag{4.39}$$

$$\sigma(t) = \dot{\sigma}(t-ts)\, ts + \sigma^*(t) \tag{4.40}$$

4. Using the equations described in section 2.2, the 3DOF equations for the RLV, the calculations for the real $\dot{h}(t)$, $\dot{\phi}(t)$, $\dot{\theta}(t)$, $\dot{v}(t)$, $\dot{\gamma}(t)$ and $\dot{\psi}(t)$ are made:

The subscript ”*” represents the reference trajectory being it the estimate data obtained in section 4.1.

With the cycle on which each variable is calculated through time fully explained, the controller test to verify how well it actuates to disturbances can begin. In the next chapter such discussion will be presented.

Chapter 5

H_∞ Optimal Controller Results

In this chapter, the controller results on how it corrected the RLV's trajectory will be showed and conclusions will be taken regarding how robust and optimal it is.

The first part of this section will address the true system equations of the RLV, that is, the system on with the disturbance will be acted on. This disturbance represents what can happen in a real descend, in which trajectory deviations due, for example, to temperature and density variations throughout the atmosphere can occur.

In the second part of this section the graphics which represent the action of the controller will be displayed, already with the action of the disturbance w and with the controller's action to achieve stabilization. Each variable of the output vector will have its graph in order to fully analyze the controller's influence.

5.1 The RLV descent system, with disturbance w

As described in the previous chapter, the system of the RLV can be described through the eq. (4.9) if there is no disturbance being absorbed by the system.

Considering w as the disturbance signal, the standard system with disturbance would be:

$$\Sigma(t) = \begin{cases} \dot{x}(t) = A(t)x(t) + B(t)u(t) + \zeta(t)w(t) \\ y(t) = E(t)x(t) \end{cases} \tag{5.1}$$

being w a matrix with the same dimensions as the matrix M and only composed by zeros, except for the columns representing the injection of disturbance into the system:

$$w = \begin{bmatrix} 0 & ... & w_h(t_l) & ... & w_h(t_n) & ... & 0 \\ 0 & ... & w_\phi(t_l) & ... & w_\phi(t_n) & ... & 0 \\ 0 & ... & w_\theta(t_l) & ... & w_\theta(t_n) & ... & 0 \\ 0 & ... & w_v(t_l) & ... & w_v(t_n) & ... & 0 \\ 0 & ... & w_\gamma(t_l) & ... & w_\gamma(t_n) & ... & 0 \\ 0 & ... & w_\psi(t_l) & ... & w_\psi(t_n) & ... & 0 \end{bmatrix} \tag{5.2}$$

being "l" and "n" representations of the time where the disturbance is being injected.

There is however an alteration made in this standard system. Given the fact that the state vector variation $\dot{x}(t)$ is used through trapezoidal and Euler integration method to calculate the $h(t)$, $\phi(t)$, $\theta(t)$, $v(t)$, $\gamma(t)$ and $\psi(t)$ as it is explained in the itemization of section 4.4, the disturbance matrix $w(t)$ must be injected later in the algorithm.

Following the thoughts taken in the before-mentioned itemization the disturbance will be injected in the following way:

$$\dot{\boldsymbol{h}}\boldsymbol{(t)} = w_h(t) + v(t)\ sin(\gamma(t)) \tag{5.3}$$

$$\dot{\boldsymbol{\phi}}\boldsymbol{(t)} = w_\phi(t) + \frac{v(t)\ cos(\gamma(t))\ cos(\psi(t))}{r(t)} \tag{5.4}$$

$$\dot{\boldsymbol{\theta}}\boldsymbol{(t)} = w_\theta(t) + \frac{v(t)\ cos(\gamma(t))\ sin(\psi(t))}{r(t)\ cos(\phi(t))} \tag{5.5}$$

$$\dot{\boldsymbol{v}}\boldsymbol{(t)} = w_v(t) - \frac{D(t)}{m} - g(t)\ sin(\gamma(t)) \tag{5.6}$$

$$\dot{\boldsymbol{\gamma}}\boldsymbol{(t)} = w_\gamma(t) + \frac{L(t)\ cos(\sigma(t))}{v(t)\ m} - \frac{g(t)}{v(t)}\ cos(\gamma(t)) + \frac{v(t)}{r(t)}\ cos(\gamma(t)) \tag{5.7}$$

$$\dot{\boldsymbol{\psi}}\boldsymbol{(t)} = w_\psi(t) + \frac{L(t)\ sin(\sigma(t))}{m\ v(t)\ cos(\gamma(t))} + \frac{v(t)}{r(t)}\ cos(\gamma(t))\ sin(\psi(t))\ tan(\phi(t)) \tag{5.8}$$

being $w_h(t)$ the disturbance subjected directly to the RLV's altitude - h. The same reasoning can be followed with the remaining disturbances.

With the disturbance system fully described, the integrity tests on the controller can begin, being the next subsections dedicated to such matter. Additionally, a flowchart was created to fully explain all the methodology used throughout the dissertation, being available in the Appendix A.

5.2 Graphics Obtained

5.2.1 RLV's Descent with no disturbance

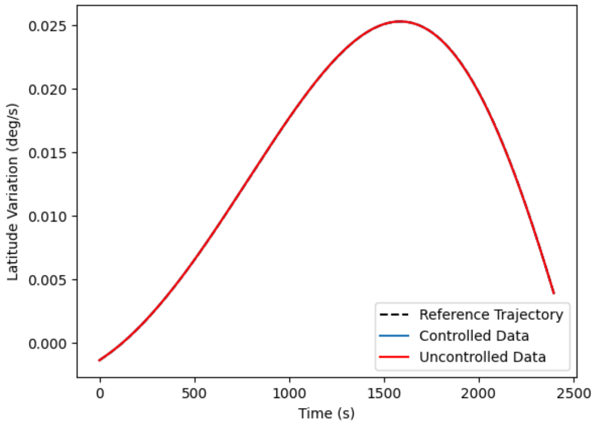

Figure 5.1: RLV's latitude development with no disturbance

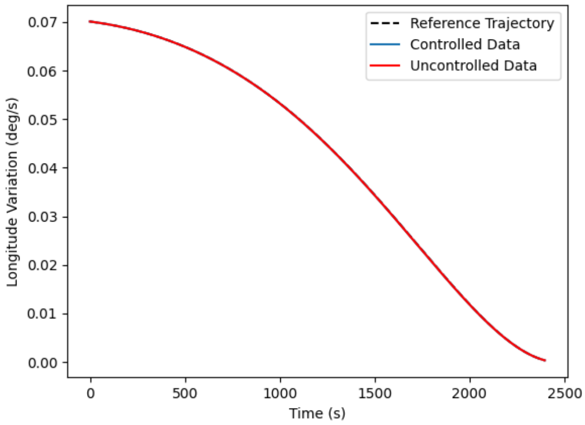

Figure 5.2: RLV's longitude development with no disturbance

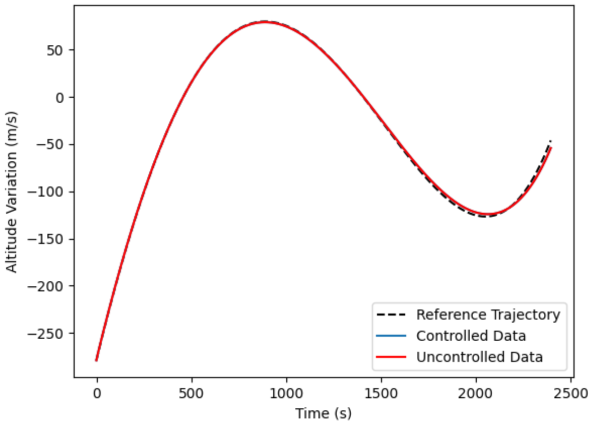

Figure 5.3: RLV's altitude development with no disturbance

5.2.2 RLV's descent with 1 disturbance

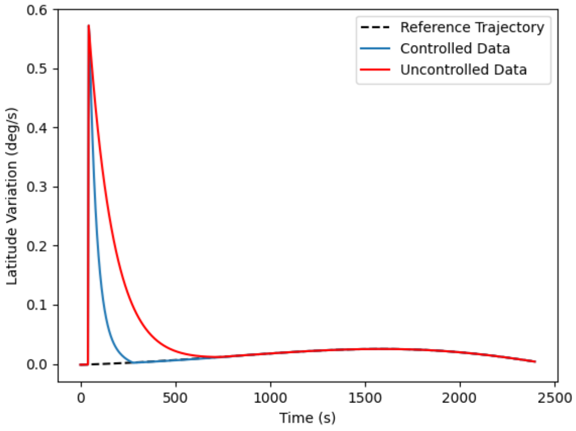

Figure 5.4: RLV's latitude development with one disturbance

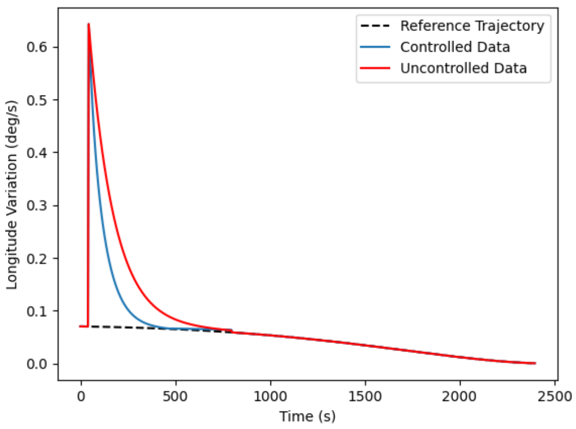

Figure 5.5: RLV's longitude development with one disturbance

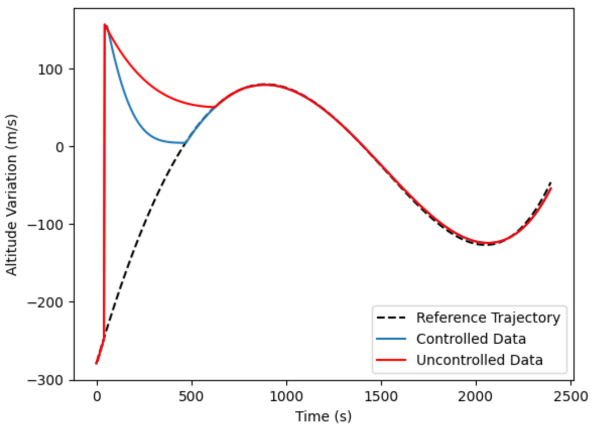

Figure 5.6: RLV's altitude development with one disturbance

Closing up for a better view of the controller actuation:

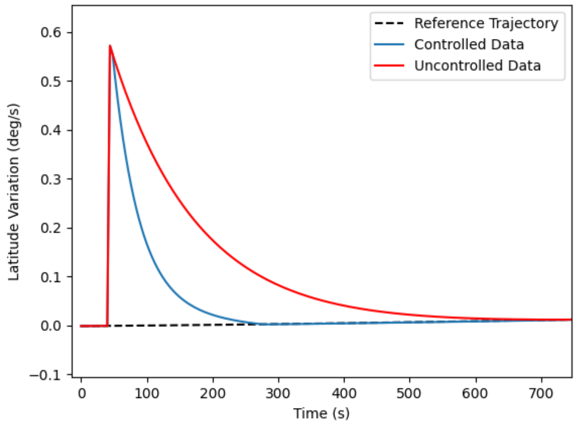

Figure 5.7: Close up to RLV's latitude first disturbance

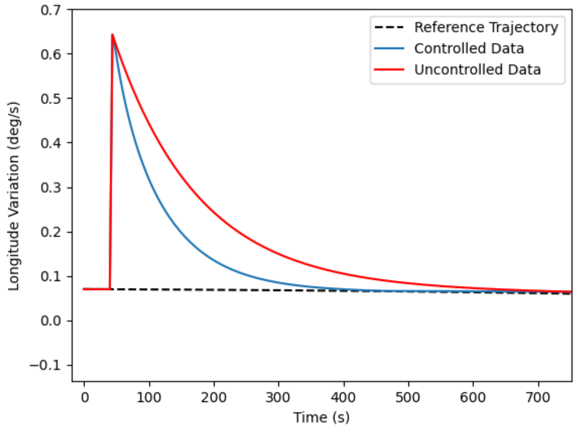

Figure 5.8: Close up to RLV's longitude first disturbance

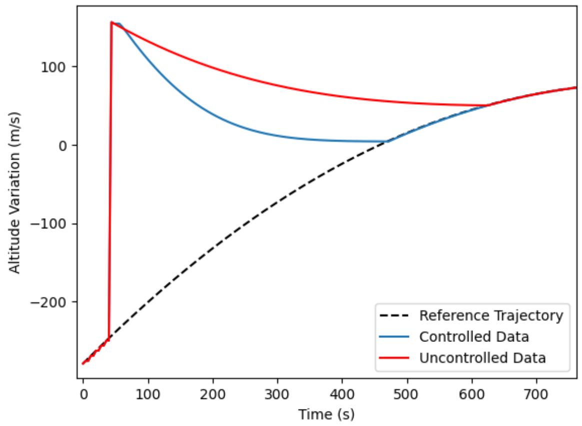

Figure 5.9: Close up to RLV's altitude first disturbance

5.2.3 RLV's descent with 2 disturbances

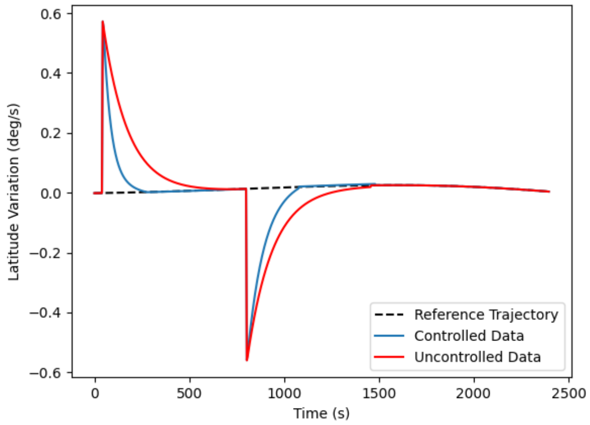

Figure 5.10: RLV's altitude development with two disturbances

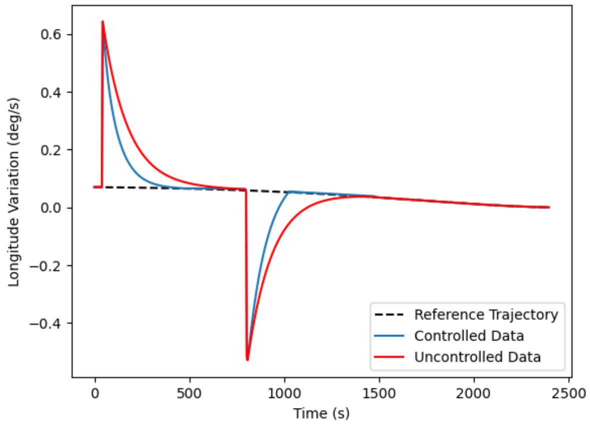

Figure 5.11: RLV's altitude development with two disturbances

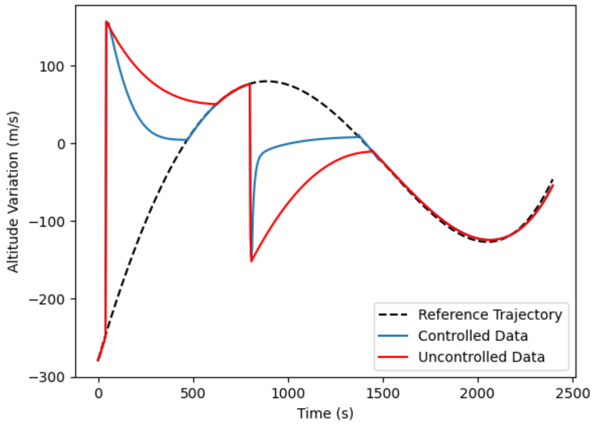

Figure 5.12: RLV's altitude development with two disturbances

Closing up for a better view of the controller actuation:

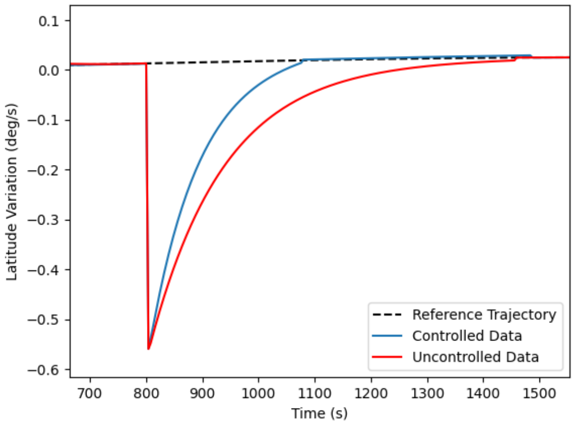

Figure 5.13: Close up to RLV's latitude second disturbance

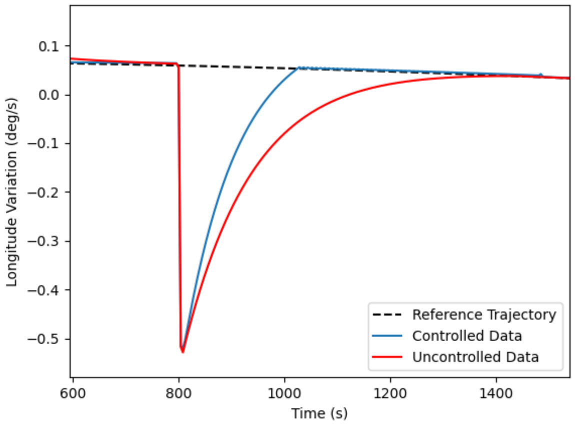

Figure 5.14: Close up to RLV's longitude second disturbance

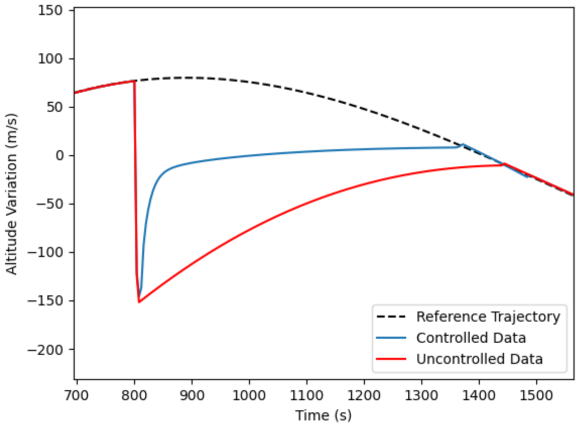

Figure 5.15: Close up to RLV's altitude second disturbance

5.2.4 RLV's descent with 3 disturbances

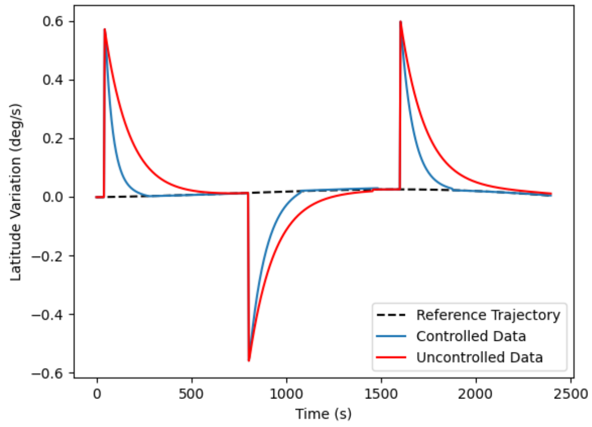

Figure 5.16: RLV's latitude development with three disturbances

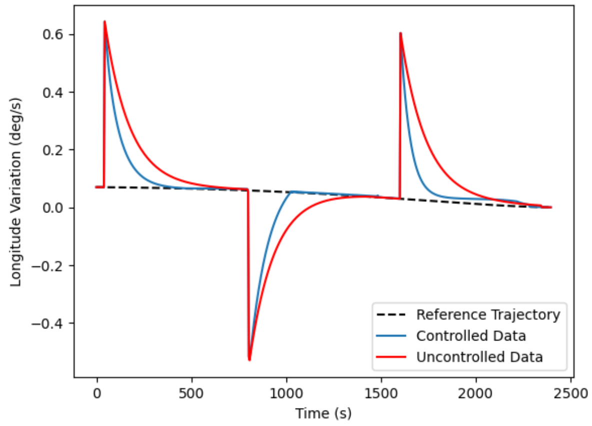

Figure 5.17: RLV's longitude development with three disturbances

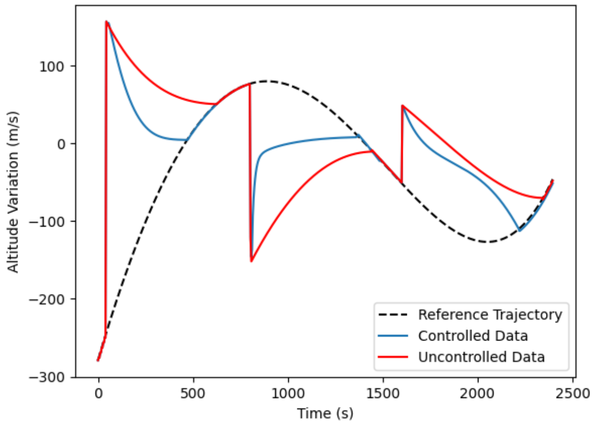

Figure 5.18: RLV's altitude development with three disturbances

Closing up for a better view of the controller actuation:

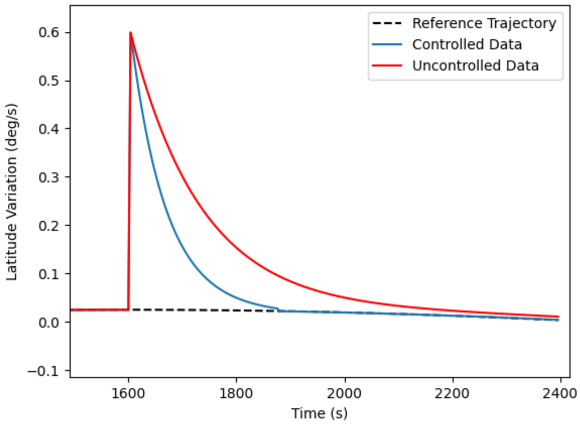

Figure 5.19: Close up to RLV's latitude third disturbance

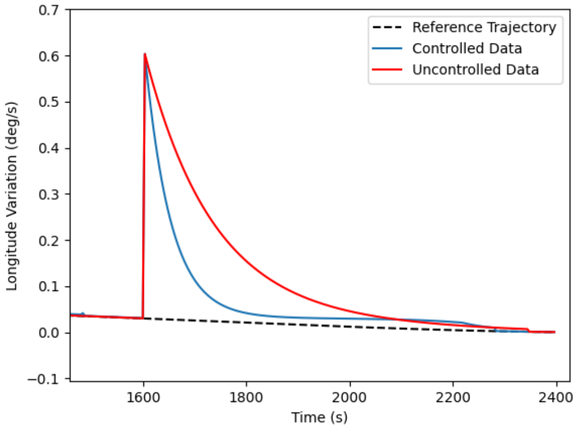

Figure 5.20: Close up to RLV's longitude third disturbance

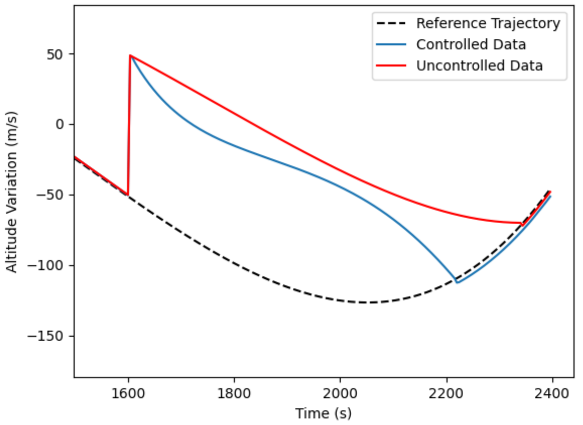

Figure 5.21: Close up to RLV's altitude third disturbance

5.3 Discussion of results

Firstly, it is important to remind the reader that the variables presented are the variations of the position vector, that is: $[\dot{\phi}, \dot{\theta}, \dot{h}]$ and not the normal variables $[\phi, \theta, h]$. By correcting a variation of the position vector, we are not only correcting the position of the vehicle but assuring that the restrictions imposed such as the heating rate, dynamic pressure and maximum deceleration are respected.

Converging the values of these variables to the desired values of the trajectory is then the same as ensuring the well-being of the RLV and its crew while guaranteeing the accomplishment of the mission. For example: if the vehicle suffers a disturbance that critically changes its current latitude variation, the vehicle can end up landing in a completely different space than the originally desired one if the system on which the RLV's flight is based does not quickly stabilize it.

Initially, the test to verify if the dynamic linearized system could follow the desired trajectory was made in subsection 5.2.1 and it was successful. The only graph that slightly showed some differences was the altitude one in fig. (5.3) at the end of the graph. That difference was in my opinion due to lack of calculation precision as naturally happens in cases where the data presented has more than 600 data points, as it happens in this project.

Given that with no disturbance present the system was capable of following and leading the shuttle into the reference trajectory, the time to test its reaction to injected disturbances began. The ”Uncontrolled Data” plot in the following graphics represents the situation in which the controller is offline ($B(t) = 0$ at all times) and the ”Controlled Data” represents the situation in which the controller is operable.

All the disturbances displayed in the graphics were artificially injected into the system as has been explained previously in this dissertation. That is the cause of their *spiky* appearance rather than a more natural disturbance.

In the subsections 5.2.2, 5.2.3 and 5.2.4 it is possible to conclude several facts, which all need to be addressed:

- As it was desirable the H_∞ produces a significant change in all three variables - $\dot{\phi}, \dot{\theta}, \dot{h}$ - but it can also be observed that it has a deeper impact on the variable $\dot{h}$ when compared to the other two variables $\dot{\phi}$ and $\dot{\theta}$;

- The state matrix of the dynamic system presented - $A(t)$ - already stabilizes the vehicle by itself, as it is verified in all the graphics shown. Regardless, the controller impacts all the graphics in a positive way making it a desirable addition to the stabilizing matrix $A(t)$ at all times.

- The third and final disturbance injected in the system $\Sigma(t)$ presented an actuation of the controller different than the remaining ones. Instead of clearly stabilizing the vehicle as in the previous cases, the altitude and longitude corrections were not ideal. That can be associated with the spikes in the final points of fig. (3.3(a)) which then produced a bad estimate in (4.3(a)).

- The controller had a different behavior on each part of the RLV decent. As stated in section 4.3, the $Q_{intensity}$ value varied in each of the disturbances to produce the results shown above. For the first disturbance, the value of this variable was 250, for the second 300 and for the final one 100.

- Finally, the controller showed effectiveness, either for a negative disturbance or a positive one, which granted even more credit to its application.

Chapter 6

Conclusions and Future Work

As stated at the end of the previous chapter, the controller was successful in stabilizing the RLV's position variation throughout its descent. However, since the state matrix is already a stabilizable one, the difference the control makes may not be as significant as in other systems that do not count on such conditions.

Furthermore, the controller was able to withstand several disturbances almost with no interval between the stabilization and the new disturbance and was capable of stabilizing each one through the vehicle's descent. This reveals the controller created in this dissertation is indeed a robust one, capable of correcting any disturbance provided to the system.

That being said, one of the possible interesting projects can be the application of this controller in a dynamic system more demanding than this one. If that application is done in a system that does not have such a stabilization provided solely by the matrix A, the actuation of the controller will have much more impact, being that situation an interesting one to observe.

In this system, the state weight matrix (Q) magnitude had to vary in time. There is not a clear explanation or reason on that matter, and such analysis could be made. It would count on the analysis of the equations entering the system at every iteration and the acknowledgment of which variables were responsible for this behavior.

Additionally, the calculation of the trajectory could be perfected. Although the trajectory used as a base to this code was a possible one, as stated by *Henrique Ferrolho* himself the trajectory he created could be more precise. Applying this controller to a trajectory made step by step could be a step forward in achieving a system with more precision and fidelity to real results, rather than using an already developed one.

The estimated functions and tools provided by *Curve Fit* were not as good as they could be. Using another function or another method different from the non-linear least-squares method could bring a more trustworthy approximation and linearization to the project, improving its precision.

Despite all these facts, the H_∞ controller was indeed successful in minimizing the difference between the present state of the vehicle and its reference state, even in a highly non-linear problem such as the one presented. It is proved that this control method is a good and trustworthy option to be responsible for the stabilization of Reentry Lifting Vehicles.

Bibliography

[1] N. Patrício, "*ESA* reúne-se em matosinhos para definir resposta a alterações climáticas e lixo espacial," *RTP Notícias*, 2021. [Online]. Available: https://www.rtp.pt/noticias/mundo/esa-reune-se-em-matosinhos-para-definir-resposta-a-alteracoes-climaticas-e-lixo-espacial_n1363758 1

[2] F. A. Administration, *Returning From Space: Re-entry*. U.S. Department of Transportation, 2011. [Online]. Available: https://www.templateroller.com/template/2129565/chapter-4-1-7-returning-from-space-re-entry.html 1, 2, 5, 18

[3] I. E. Alber, *Aerospace Engineering on the Back of an Envelope*, ser. ISBN: 978-3-642-22536-9. Springer, Praxis, 2003. [Online]. Available: https://link.springer.com/book/10.1007/978-3-642-22537-6 1, 5, 18

[4] L. C. K. D-Hicks, *Introduction to Astrodynamic Reentry*, ser. ISBN: 978-3-642-22536-9. Books Express Publishing, 2009. [Online]. Available: https://link.springer.com/book/10.1007/978-3-642-22537-6 2, 7, 13

[5] J. Dumoulin. (1998) Mission events summary. Information content from the NSTS Shuttle Reference Manual. [Online]. Available: https://science.ksc.nasa.gov/shuttle/technology/sts-newsref/sts_mes.html#mes_deorbit 2, 22, 23

[6] W. Hale, N. Aeronautics, S. Administration, H. Lane, N. Aeronautics, S. A. N. Staff, J. Young, G. P. Office, K. Lulla, R. Crippen, and G. Chapline, *Wings In Orbit: Scientific and Engineering Legacies of the Space Shuttle 1971-2010*, ser. NASA SP. NASA, 2010. [Online]. Available: https://books.google.pt/books?id=WZeXrp7uFYoC 3, 4, 7, 8

[7] J. Dumoulin. (1998) Mission profile. Information content from the NSTS Shuttle Reference Manual. [Online]. Available: https://science.ksc.nasa.gov/shuttle/technology/sts-newsref/mission_profile.html#rtls_abort 3

[8] E. M. Henderson and T. X. Nguyen, "Space shuttle abort evolution," in *AIAA Paper 2011 Conference Exposition*, ser. NASA Technical Reports. NASA, 2011. 3

[9] J. C. Adams, "Atmospheric re-entry," 2003. [Online]. Available: https://www.semanticscholar.org/paper/Atmospheric-Re-Entry-Adams/93a999c628435aeea754de8436ea0cd5dc5b09d7 5

[10] N. X. Vinh, A. Busemann, and R. D. Culp, *Hypersonic and planetary entry flight me-*

chanics. University of Michigan Press Ann Arbor, 1980. [Online]. Available: https://www.academia.edu/8611588/Hypersonic_and_planetary_entry_flight_mechanics 6, 13

[11] X. J. Jiang Zhao, Rui Zhou, "Atmospheric re-entry," *Journal of Systems Engineering and Electronics*, vol. 25, no. 4, pp. 627–639, 2014. 9, 10

[12] Y. W. Xing Wei, Lei Liu, "Reentry trajectory optimization for a hypersonic vehicle based on an improved adaptive fireworks algorithm," *International Journal of Aerospace Engineering*, 2018. 9, 15, 18

[13] G. Zifeng and Z. e. a. Hexin, "Reentry tracking control of hypersonic glider based on legendre pseudospectral method," in *2018 Chinese Control And Decision Conference (CCDC)*, 2018, pp. 1860–1864. 9

[14] Q. Hao, S. Peng, and L. Xinguo, "General reentry trajectory planning method based on improved maneuver coefficient," *IEEE Access*, vol. PP, 12 2018. 9

[15] A. Banerjee and M. Nabi, "Re-entry trajectory optimization for space shuttle using sine-cosine algorithm," in *2017 8th International Conference on Recent Advances in Space Technologies (RAST)*, 2017, pp. 73–77. 9

[16] Y. M. Lu. Wang, Qinghua Xing, "Reentry trajectory rapid optimization for hypersonic vehicle satisfying waypoint and no-fly zone constraints," *Journal of Systems Engineering and Eletronics*, vol. 26, no. 6, pp. 1277–1290, 2015. 9

[17] Earth's spherical model. [Online]. Available: https://www.gratispng.com/png-tbkf6t/ 10

[18] A. H. Marwan Bikdash, Ken Sartor, "Fuzzy guidance of the shuttle orbiter during atmospheric reentry," *Control Engineering Practice*, vol. 3, no. 7, p. 295–303, 1999. 10

[19] X. Guo, R. Qi, and X. Yao, "Predictor-corrector guidance for reentry hypersonic vehicle based on feedback linearization," in *2017 29th Chinese Control And Decision Conference (CCDC)*, 2017, pp. 6516–6521. 10

[20] T. Ye, H. Chao-fang, F. Hao, and W. Na, "Reentry guidance method based on predictive control for hypersonic vehicle," in *2017 29th Chinese Control And Decision Conference (CCDC)*, 2017, pp. 6790–6794. 10

[21] M. H. Breitner, "Robust optimal on-board reentry guidance of an european space shuttle: Dynamic game approach and guidance synthesis via neural networks," *JOURNAL OF OPTIMIZATION THEORY AND APPLICATIONS*, vol. 107, pp. 481–503, 07 2000.

11

[22] D. Abbasi and M. Mortazavi, “A new concept for atmospheric reentry optimal guidance: An inverse problem inspired approach,” *Mathematical Problems in Engineering*, vol. 2013, 01 2013. 13

[23] X. Guo, R. Qi, and X. Yao, “Predictor-corrector guidance for reentry hypersonic vehicle based on feedback linearization,” *International Journal of Aerospace Engineering*, pp. 6516–6521, 2017. 14

[24] K. Bousson, “Lecture notes of flight dynamics and control,” master’s Degree of Aeronautical Engineering. Aerospace Sciences Department at University of Beira Interior, 2019. 15, 16

[25] Aviation Performance Solutions. What is angle of attack? — three critical angles. [Online]. Available: https://www.apstraining.com/resource/three-critical-angles/ 16

[26] R. C. e. a. Ried, “Space shuttle orbiter entry heating and tps response: Sts-1 predictions and flight data,” in *Langley Research Center Computational Aspects of Heat Transfer in Struct*. NASA, 1982, pp. 327–348. 18

[27] J. T. Betts, *6. Optimal Control Examples*. siam, 2010. [Online]. Available: https://epubs.siam.org/doi/abs/10.1137/1.9780898718577.ch6 21, 22, 23

[28] I. Dunning, J. Huchette, and M. Lubin, “Jump: A modeling language for mathematical optimization,” *SIAM Review*, vol. 59, no. 2, pp. 295–320, 2017. 23

[29] M. Schmidt, “An interior-point method for nonlinear optimization problems with locatable and separable nonsmoothness,” *EURO Journal on Computational Optimization*, vol. 3, no. 4, pp. 309–348, 2015. [Online]. Available: https://www.sciencedirect.com/science/article/pii/S2192440621000496 23

[30] Henrique Ferrolho. Space shuttle reentry trajectory. [Online]. Available: https://github.com/ferrolho/space-shuttle-reentry-trajectory 24

[31] P. M. E. Broucke, “Linearization of nonlinear systems,” 2007. 36, 37

[32] P. W. et all., “Linearizing ODEs,” dec 4 2021, [Online; accessed 2021-12-12]. 36

[33] K. Iqbal, “Controller Design in Sate-Space,” mar 5 2021, [Online; accessed 2021-12-16]. 39

[34] X. Cubillos and L. Souza, “Using of h-infinity control method in attitude control system of rigid-flexible satellite,” *Mathematical Problems in Engineering*, vol. 2009, 12 2009.

39

[35] P. Apkarian and D. Noll, "The H∞ Control Problem is Solved," *Aerospace Lab*, no. 13, pp. pages 1–11, Nov. 2017. [Online]. Available: https://hal.archives-ouvertes.fr/hal-01653161 39

[36] P. Khargonekar, I. Petersen, and M. Rotea, "H/sub infinity /-optimal control with state-feedback," *IEEE Transactions on Automatic Control*, vol. 33, no. 8, pp. 786–788, 1988. 40, 41

[37] B. Francis, *A Course in H Infinity Control Theory*, ser. Lecture notes in control and information sciences. Springer, 1987. [Online]. Available: https://books.google.pt/books?id=O9ZCswEACAAJ 41

[38] C. A. Thompson, "A study of numerical integration techniques for use in the companion circuit method of transient circuit analysis." Purdue University School of Electrical Engineering, 1992. 43

Appendix A

Flowchart of The Dissertation Algorithm

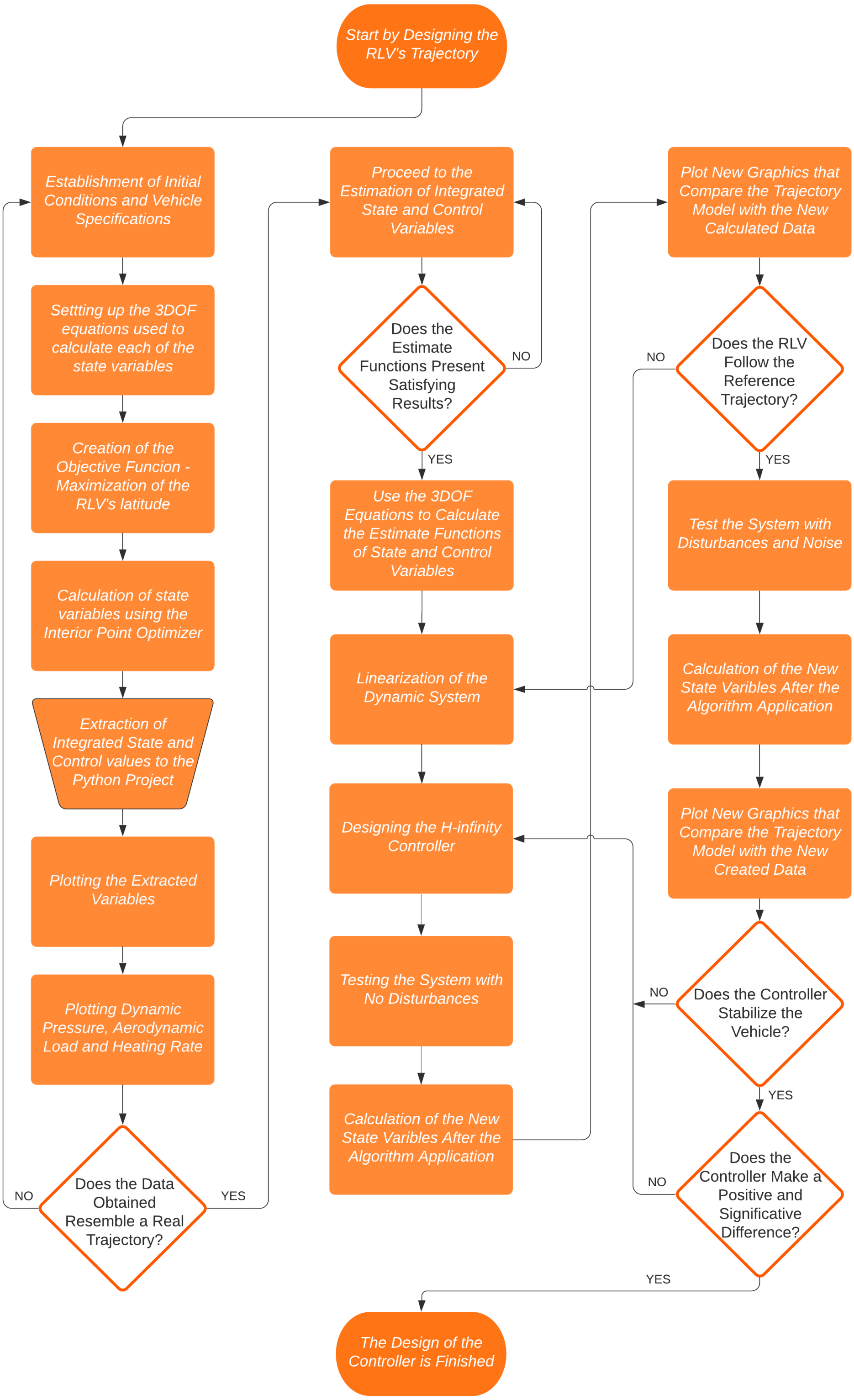
Start by Designing the RLV's Trajectory
Establishment of Initial Conditions and Vehicle Specifications
Settting up the 3DOF equations used to calculate each of the state variables
Creation of the Objective Funcion - Maximization of the RLV's latitude
Calculation of state variables using the Interior Point Optimizer
Extraction of Integrated State and Control values to the Python Project
Plotting the Extracted Variables
Plotting Dynamic Pressure, Aerodynamic Load and Heating Rate
Does the Data Obtained Resemble a Real Trajectory?
NO
YES
Proceed to the Estimation of Integrated State and Control Variables
Does the Estimate Functions Present Satisfying Results?
NO
YES
Use the 3DOF Equations to Calculate the Estimate Functions of State and Control Variables
Linearization of the Dynamic System
Designing the H-infinity Controller
Testing the System with No Disturbances
Calculation of the New State Varibles After the Algorithm Application
Plot New Graphics that Compare the Trajectory Model with the New Calculated Data
Does the RLV Follow the Reference Trajectory?
NO
YES
Test the System with Disturbances and Noise
Calculation of the New State Varibles After the Algorithm Application
Plot New Graphics that Compare the Trajectory Model with the New Created Data
Does the Controller Stabilize the Vehicle?
NO
YES
Does the Controller Make a Positive and Significative Difference?
NO
YES
The Design of the Controller is Finished

Appendix B

Academic Article - Versão Corrigida após defesa

This page was purposely left in blank. The academic Article begins in the next page.

Journal ....., Vol. xxx, No. 1, 1-5, 2021
Additional note

Optimal and Robust Control of Atmospheric Reentry Trajectories
(Preliminary Version, to be submitted)

António Moreira[1]*, Kouamana Bousson[2]*

Abstract

Reentering the Earth's atmosphere is one of the most difficult phases of any spaceship's mission. During reentry, following an optimal trajectory in terms of minimal heating rate, dynamic pressure, and maximum deceleration is vital to the mission's success. This paper proposes a novel design for a controller based on H_∞ control methods, with the goal of achieving optimal and robust control for a Reentry Lifting Vehicle. This paper begins by summarizing the theory and history behind the Shuttle Space Program, including the planning of its trajectories and descriptions of the Reentry Flight Dynamics Model. The analysis of the reference trajectory obtained will follow and the comparison of it to a real shuttle trajectory will be made. The design and configuration of the H_∞ controller comes after, beginning with the linearization of the system obtained in the previous step and ending with the recalculation of vehicle state variables after its application. The disturbance is then applied and the results of the actuation of the controller are displayed. The H_∞ controller for Reentry Lifting Vehicle proves itself to be a useful application presenting satisfying and significant results in this critical phase of flight.

Keywords

Optimal and Robust Control — Reentry Lifting Vehicle — H_∞ Control Method

[1] *MSc Student, Aerospace Science Department, University of Beira Interior, Covilhã, Portugal*
[2] *Professor, Aerospace Science Department, University of Beira Interior, Covilhã, Portugal*
***Corresponding author**: bousson@ubi.pt

Contents

Introduction

Adventuring into space has been for a long time an accomplished dream of mankind. While exiting the atmosphere is itself a challenge, being capable of safely landing and reentering the atmosphere with a manned space aircraft is an even heavier challenge. Throughout the years, numerous satellites have been launched into the atmosphere with no plan of return, becoming sooner or later disposable material continuously in orbit. Guaranteeing the safe return of the no-longer-used satellites and spacecraft is a critical mission if we want to leave our atmosphere as clean as possible. According to *Portugal Space*: ”every year approximately 100 tons of uncontrolled debris reenter Earth's atmosphere, a situation that explains the urgency of developing technology and solutions that allow the controlled and safe removal of this debris that humanity left in space” [1].

Reentering the atmosphere is then the most critical part of the mission of a shuttle or any similar spaceship. From an astronaut's point of view, the atmosphere presents a dense fluid, which at orbital velocities, is not that far from the surface of a lake [2]. The trajectory followed must allow the minimum temperature peaks considering the aerodynamic heating along the way to ensure the integrity of the shuttle and no loss of materials during the reentry. The tragedy of Columbia (STS-107) is a fatal reminder of the dangerous thermal and aerodynamic environment that any vehicle reentering the atmosphere endures [3].

The design and calculation of the reentry trajectory can be summarized in 3 competing requirements: deceleration limits, heating limits, and impact/landing accuracy [4]. The materials used in the vehicle directly impact the maximum deceleration it can endure. Considering g as a deceleration unit and g being the gravitational acceleration at sea level ($9,80665\ m/s^2$), the material's used for the RLV structure must be capable of enduring the maximum g's the vehicle will be subjected to. Since in this paper the RLV is carrying human life, the maximum value of deceleration will be 12 g's - value for the maximum deceleration humans can with-take [2]. The heating is also a noticeable problem. The friction between the air and the RLV traveling at thousands of meters per second drastically increases the temperature of its materials. The normal temperature throughout the reentry as well as the peak temperature of the shuttle must be studied, given the fact that it can reach values of $1648°C$ [5]. The accuracy of landing or impact is the last component considered, being it determined according to the type of mission. This component is critical in the case of this paper considering the RLV should land on a controlled and prepared runway.

A typical shuttle trajectory is limited by two situations: the undershoot and the overshoot boundary. The limit on which the deceleration and heating rate is impossible to withstand, being that from the crew or the vehicle represents the undershoot boundary. On the other hand, the limit on which the vehicle will not initiate the reentry phase due to the small gravitational force encountered when compared to the momentum of the vehicle, represents the overshoot trajectory [6]. These two situations form the reentry corridor, where the trajectory of this paper must belong in order to safely land the shuttle. After entering Earth's atmosphere the shuttle must decelerate and start descending through the atmosphere. To do so, the angle of attack (AoA) and the bank angle of the RLV must be controlled throughout its descend - the use of the AoA allows the deceleration of the RLV through the generation of aerodynamic drag, while the bank angle allows the descend of the RLV by decreasing the aerodynamic lift produced in the generation of aerodynamic drag [7].

Throughout the years, researchers have been looking for ways to develop a control system capable of stabilizing the RLV, returning it to the reference trajectory regardless of the disturbances suffered during its descend. Marwan Bikdash et al. designed a fuzzy guidance for the shuttle orbiter during atmospheric reentry [8]. Making use of *Sugeno* approximations, the authors trained hybrid fuzzy-crisp interference systems with examples of past reentries. A predictor-corrector reentry guidance was proposed by Xiaoping Guo et al. in [9] based on Feedback Linearization to reduce the difference between reference trajectory and the RLV current state after an applied disturbance. The authors used the Quasi Equilibrium Glide Condition as another constraint and controlled the vehicle with the same control variables as in this paper - α and σ. M. H. Breitner made use of *Rufus Philip Isaacs* nonlinear first-order partial differential equations to set up interior and boundary conditions, being the restrictions to the RLV similar to this paper [10]. The algorithm presented satisfying results and proved real-life applicability in its theory and numerical methods.

The objective of this paper is to create an optimal H_∞ control which ensures the maneuverability of a reentry lifting vehicle and its control throughout its reentry. The controller must guarantee that the vehicle reentering the atmosphere follows the trajectory desired, even when subjected to noise and disturbances during its flight. Furthermore, it is desirable for the controller to be robust which implicates the capability of stabilizing the vehicle regardless of the number of disturbances applied and their magnitude.

1. Reentry Flight Dynamics Model

In this section the possible assumptions that can be made when we estimate the optimal trajectory of reentry will be explained. Furthermore, the Reentry dynamics equations will be presented as well as the equations used to calculate the maximum value for the constraints of the presented problem.

1.1 Assumptions Made

One of the most important assumptions made is the use of the spherical model of the Earth in the calculations of the reentry trajectory. It is a known factor that Earth has an elliptical form which can be observed by the cross-section of all the meridians. However, the benefits obtained by considering the Earth as a spherical body significantly justify the precision lost in the procedure as was made in [11, 12, 13].

Regarding Earth's rotation, there are two decisions that can be made: consider earth as a rotating body or as a stationary body. Considering the Earth's rotation as part of the equations, despite adding slightly more precision to the final results the outstanding difference in algorithm complexity makes the decision of considering the Earth as a stationary Body a viable decision, as was used in [13, 14, 15]. With these facts in mind, the method followed in this dissertation was the spherical non-rotating Earth.

Figure 1. Earth as a Spherical Model [16].

1.2 Coordinate Frame

The coordinate system used for this dissertation will be a Planet-Fixed frame. Firstly, it is designed a Geocentric Equatorial Coordinate Frame where its origin resides in the center of motion (COM) of the planet Earth. Its axis X will be directed to the Greenwich Meridian and the axis Y will be directed such that it lies in the equatorial plane and makes a 3-axis system with the axis X and Z with a 90° angle between each one [4, 6, 17]. The coordinate system can be seen in fig. (2):

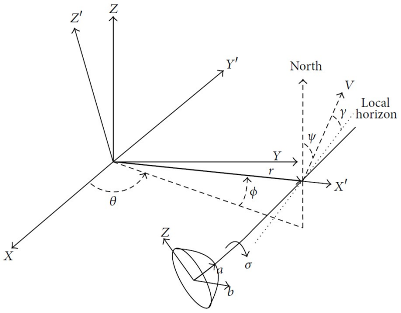

Figure 2. Coordinate Frame. [17]

where r represents the distance between the COM of the planet and the COM of the reentering vehicle. The longitude will then be represented by θ and the latitude by ϕ.

The symbol σ represents the angle between the vehicle longitudinal symmetry plane and the vertical plane, otherwise known as the bank angle and γ represents the velocity flight angle.

The letter V represents the velocity vector of the vehicle at a given moment in time and ψ is the heading angle measured from North.

Throughout this work, h will sometimes be used instead of r, while the only difference between these two variables is the Earth's radius - $r = h + R$ -, being R the Earth's medium radius.

1.3 Reentry Dynamics

The 3DOF equations of a hypersonic vehicle reentering the atmosphere consider earth as a spherical and non-rotating body, and are shown as in [18]:

$$\dot{h} = v\, sin(\gamma) \tag{1}$$

$$\dot{\phi} = \frac{v\, cos(\gamma)\, cos(\psi)}{r} \tag{2}$$

$$\dot{\theta} = \frac{v\, cos(\gamma)\, sin(\psi)}{r\, cos(\phi)} \tag{3}$$

$$\dot{v} = \frac{-D}{m} - g\, sin(\gamma) \tag{4}$$

$$\dot{\gamma} = \frac{L\, cos(\sigma)}{v\, m} - \frac{g}{v}\, cos(\gamma) + \frac{v}{r}\, cos(\gamma) \tag{5}$$

$$\dot{\psi} = \frac{L\, sin(\sigma)}{m\, v\, cos(\gamma)} + \frac{v}{r}\, cos(\gamma)\, sin(\psi)\, tan(\phi) \tag{6}$$

where v stands for the velocity relative to Earth as a scalar. The other variables were already explained in the previous sub-section. Earth's gravity acceleration is represented by the letter g and it's calculated according to the RLV's altitude h:

$$g = g_0 \left(\frac{R}{R+h}\right)^2 \tag{7}$$

where g_0 is the gravity Acceleration at sea level.

Since the vehicle is an RLV, it will be subjected to both aerodynamic forces of lift L and drag D which can be calculated as follows:

$$L = \frac{1}{2}\, \rho\, v^2\, S\, C_L\, (\alpha, M_a, \sigma, \delta_e) \tag{8}$$

$$D = \frac{1}{2}\, \rho\, v^2\, S\, C_D\, (\alpha, M_a, \sigma, \delta_e) \tag{9}$$

where S is the reference area of the RLV and m the reference of its mass. C_L and C_D being the lift and drag coefficient, respectively, and will be calculated according to the AOA - α -, bank angle σ, elevator angle δ_e and Mach number $M_a = \frac{v}{sound\ velocity}$. The atmospheric density ρ is calculated by:

$$\rho = \rho_0\, exp\left(-\frac{h}{h_s}\right) \tag{10}$$

where ρ_0 is the atmospheric density at sea level, h is the current altitude of the vehicle when compared to the sea level and h_s is the scalar height coefficient [11].

The lift and drag coefficient can be calculated as in [19]:

$$C_L = C_{L0} + C_{L\alpha}\, \alpha + \frac{\bar{c}}{2V}\, \left(C_{L\dot{\alpha}}\, \dot{\alpha} + C_{Lq_p}\, q_p\right) + C_{L\delta_e}\, \delta_e \tag{11}$$

$$C_D = C_{D0} + C_{D\alpha}\, \alpha + \frac{\bar{c}}{2V}\, \left(C_{D\dot{\alpha}}\, \dot{\alpha} + C_{Dq_p}\, q_p\right) + C_{D\delta_e}\, \delta_e \tag{12}$$

where q_p represents the pitch rate and α the AOA. C_L and C_D are calculated by several parts:

- C_{L0} and C_{D0} are related to the RLV body;
- $C_{L\alpha}$ and $C_{D\alpha}$ are related to the current AOA;
- $C_{L\delta_e}$ and $C_{D\delta_e}$ are related to the elevator's deflection.

To calculate the pitch rate, we first need to clarify the reasoning behind it. Considering the letter λ as the pitch angle, the following assumption can be made:

$$\lambda = \alpha + \gamma \tag{13}$$

that is, the pitch angle is the sum of the AOA - α - and the flight path angle - γ - which can be visualized in fig. (3).

With the value of the pitch angle λ, it is now possible to get the value of the pitch rate q by use of the following equation found in [19]:

$$\dot{\lambda} = q\, cos(\sigma) - h\, sin(\sigma) \tag{14}$$

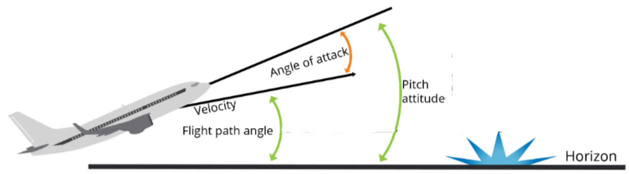

Figure 3. Representation of an Aircraft's Pitch Angle, adapted from [20].

Isolating q_p and deriving the eq. (13) it is now possible to calculate the pitch rate as:

$$q_p = \frac{h\,sin(\sigma) + \dot{\alpha} + \dot{\gamma}}{cos(\sigma)} \tag{15}$$

1.4 State Vector

To estimate the trajectory, the state vector of the RLV must describe its condition throughout all reentry phases. Based on the flight dynamics equations, the state vector of the vehicle can be described as:

$$x = \begin{bmatrix} \dot{h} \\ \dot{\phi} \\ \dot{\theta} \\ \dot{v} \\ \dot{\gamma} \\ \dot{\psi} \end{bmatrix} \tag{16}$$

where $[\dot{r}, \dot{\phi}, \dot{\theta}]$ represent the vector of position variation in spherical coordinates and $[\dot{v}, \dot{\gamma}, \dot{\psi}]$ represent the vector of velocity variation, also in spherical coordinates:

- $\dot{h}$ – altitude variation of the RLV
- $\dot{\phi}$ – latitude variation of the RLV
- $\dot{\theta}$ – longitude variation of the RLV
- $\dot{v}$ – velocity variation of the RLV
- $\dot{\gamma}$ – flight path angle variation of the RLV
- $\dot{\psi}$ – heading angle variation of the RLV

With these variables in the state vector, the projection of the controller and the constant monitoring of its flight throughout all phases of flight becomes possible.

1.5 Applied Constraints

The constraints used to limit the presented problem were inspired by the work developed in [2, 3, 11, 21].

1.5.1 Heating Rate

$\dot{Q}_s$ is the heating rate of the vehicle at a certain point, which must be limited by the maximum heating rate the vehicle can endure and is calculated by:

$$\dot{Q}_s \cong k_Q\, v^3 \sqrt{\frac{\rho}{r_{nose}}} \leq \dot{Q}_{s_{max}} \tag{17}$$

where k_Q is the heating rate normalization constant, r_{nose} is the vehicle's nose radius and $\dot{Q}_{s_{max}}$ is the maximum heating rate the vehicle can withstand. The value k_Q = $1,75E-04\sqrt{kg/m}$ was used as in [3].

1.5.2 Dynamic Pressure

Dynamic pressure presents itself with the letter q and it is limited to control the hinge moment of an actuator in a determined range. The dynamic pressure must be less than a certain maximum value, and it is calculated by:

$$q = \frac{1}{2}\,\rho\, v^2 \leq q_{max} \tag{18}$$

1.5.3 Maximum Deceleration

There will be a limit to how much deceleration will the vehicle be subjected to. The maximum deceleration a human can withstand is 12 $g's$. However, it will be limited to 3 $g's$ not only for structural reasons but for the comfort and well-being of the RLV's crew.

The deceleration is calculated as:

$$a = \frac{v^2\,\omega\,sin(\gamma)}{2e} \leq a_{max} \tag{19}$$

where ω represents the atmospheric scaled height, a parameter used to describe the density profile of the atmosphere. The letter e represents the base of the natural logarithm [2].

1.5.4 Controllability of the RLV

To ensure the controllability of the RLV we must ensure that the AoA, bank angle, elevator and rudder angle stay within certain limits:

$$\alpha_{min} \leq \alpha \leq \alpha_{max},\ |\dot{\alpha}| \leq \dot{\alpha}_{max} \tag{20}$$

$$\sigma_{min} \leq \sigma \leq \sigma_{max},\ |\dot{\sigma}| \leq \dot{\sigma}_{max} \tag{21}$$

$$\delta_{emin} \leq \delta_e \leq \delta_{emax},\ |\dot{\delta}_e| \leq \dot{\delta}_{emax} \tag{22}$$

being $\dot{\alpha}_{max}, \dot{\sigma}_{max} \leq 5°/s$, $\alpha_{min} = 0°$, $\alpha_{max} = 60°$, $\sigma_{min} = -89°$ and $\sigma_{max} = 90°$.

With the above-mentioned restrictions, we form our entry corridor on which we will find the optimal trajectory for the RLV and then project the controller for it.

1.6 Output Vector

The output vector will be composed with the Geodetic Coordinates Variation - $\dot{\phi}$, $\dot{\theta}$ and $\dot{h}$ - making it possible to transform them into Geodesic coordinates if there is a desire to do so.

The output vector will then be as follows:

$$y = \begin{bmatrix} \dot{\phi} \\ \dot{\theta} \\ \dot{h} \end{bmatrix} \tag{23}$$

2. Reentry Trajectory Analysis

This chapter will consist on the analysis of the trajectory on which the controller will be designed. To ensure the validity of the controller that will be developed, this trajectory must resemble one of a real shuttle and follow the dynamics and restrictions explained throughout the previous sections.

As the objective of this paper is not to develop a trajectory but to develop an optimal and robust controller that could be implemented on the RLV's software, the possibility to use an adequate trajectory already developed surged. Such trajectory was found and created by *Henrique Ferrolho* and it was initially inspired in the problem suggested in chapter 6 of "Practical Methods for Optimal Control and Estimation Using Nonlinear Programming" by *John T. Betts* [22].

2.1 Trajectory Estimation as an Optimal Control Problem

Designing the best possible reentry trajectory for a shuttle is a highly nonlinear estimation problem. The nonlinear behavior of this problem makes the use of a simple shooting method impossible. *John T. Betts* presents a possible way to solve this problem, using the same reentry flight dynamics presented in (section 1.3).

2.1.1 Objective Function

To reach the solution of the problem the need to set an objective function existed. For the presented paper, the objective function will be the maximization of the cross-range of the RLV.

$$J = \phi(t_f) \tag{24}$$

in which J represents the objective function. Maximizing the cross-range of the vehicle is the same as maximizing the final latitude of the RLV, hence the transformation to ϕ in the previous formula.

2.1.2 Initial conditions, RLV's characteristics and Final conditions

The initial conditions to the problem were first described in [22]:

Variables	Values
h_i	$400.000\ ft$
ϕ_i	$0\ \ deg$
θ_i	$0\ deg$
v_i	$25.600\ ft/s$
γ_i	$-1,1\ deg$
ψ_i	$90\ deg$
h_i	$121.920\ m$
ϕ_i	$0\ rad$
θ_i	$0\ rad$
v_i	$7.802,88\ m/s$
γ_i	$-0,0192\ rad$
ψ_i	$1,5708\ rad$

Table 1. Initial Conditions in Imperial and SI units

with the following RLV characteristics and subjected to the following earth acceleration:

$$m = 203.000\ lb$$
$$S = 2.690\ ft^2$$
$$g_0 = 32,174\ ft/s^2$$
$$m = 92.079,251\ kg$$
$$S = 249,91\ m^2$$
$$g_0 = 9,8066\ m/s^2$$

Table 2. RLV's Characteristics in SI units

As mentioned before the reentry trajectory will end with the start of the TAEM phase which will start when the vehicle reaches the following numbers:

$$h_f = 80.000\ ft$$
$$v_f = 500\ ft/s$$
$$\gamma_f = -5\ deg$$
$$h_f = 24.384\ m$$
$$v_f = 152,4\ m/s$$
$$\gamma_f = -0,0873\ rad$$

Table 3. Final Conditions in imperial and SI units

2.2 Algorithm of the Reference Reentry Trajectory

An open MIT licensed code capable of calculating an estimate trajectory was found. In this code, *Henrique Ferrolho* solved the exact problem of chapter 6 from [22] with the help of *JuMP*, a specific domain that belongs to *Julia*'s programming language.

The optimizer used to find the solution to the reentry trajectory problem was the interior-point optimizer. This optimizer is widely used in many different problems being capable of solving linear and nonlinear problems, according to the user's needs.

Briefly explaining the code, the optimizer starts at the initial conditions described in 2.1.2 and varies each parameter from the vehicle's state vector in a time step of 4 seconds, with the objective of maximizing the final cross range of the RLV's until the final conditions are reached. For each time step, an array for that specific time is being created such as:

$$x(t_k) = \begin{bmatrix} \dot{h}(t_k) \\ \dot{\phi}(t_k) \\ \dot{\theta}(t_k) \\ \dot{v}(t_k) \\ \dot{\gamma}(t_k) \\ \dot{\psi}(t_k) \end{bmatrix} \tag{25}$$

Using as control variables the following array:

$$u(t_k) = \begin{bmatrix} \dot{\alpha}(t_k) \\ \dot{\sigma}(t_k) \end{bmatrix} \tag{26}$$

where k represents the current cycle of the code. Compiling the arrays in a matrix will then allow the full study of the reentry trajectory of the vehicle and the projection of the code for the optimal controller.

In each step of the code the variables calculated were integrated resulting in the values of altitude, latitude, longitude, velocity, flight path angle, heading angle, angle of attack, and bank angle of the RLV:

$$\bar{x}(t_k) = \begin{bmatrix} h(t_k) \\ \phi(t_k) \\ \theta(t_k) \\ v(t_k) \\ \gamma(t_k) \\ \psi(t_k) \end{bmatrix} \tag{27}$$

$$\bar{u}(t_k) = \begin{bmatrix} \alpha(t_k) \\ \sigma(t_k) \end{bmatrix} \tag{28}$$

The code produced by *Henrique Ferrolho* can be found in [23] and is totally open for public use, being it as it is presented, or to change it in any way the user pleases. As stated before, the used code had some alterations when compared to the original one, since some of the constant values used in the original were not a match to a real shuttle as was explained in 2.1.2.

2.3 Linearization of the system and H_∞ Setup

Despite the fact that this system is a highly-nonlinear one, it is possible to approximate it to a rather linear behavior within a certain operating range of an equilibrium point, as stated in [24]. The calculation of equilibrium points is made by fixing a given $u = u^*$ and calculating the respective equilibrium state $x = x^*$ - which becomes the equilibrium point.

$$\Sigma = \begin{cases} \dot{x}(t) = A(t)x(t) + B(t)u(t) \\ y(t) = Ex(t) \end{cases} \tag{29}$$

where A is the state matrix, B the control matrix and E the output matrix. With the system fully linearized it is possible to start the setup of the H_∞ method controller.

The H_∞ methods are considered in control theory a fine solution to create controllers in which stabilization of the system is achieved with great performance. It has had a great impact on the development of control systems throughout the decades of 1980 and 1990 [25]. This method is then used for cases when the objective is to achieve a robust and optimal controller, as it happens in this paper.

The functioning of the H_∞ controller can be theoretically visualized in [26]:

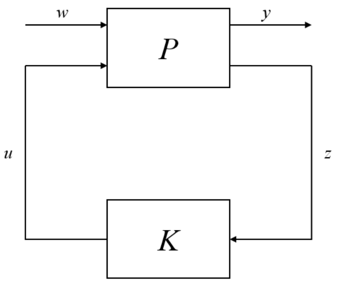

Figure 4. H_∞ Method Block Diagram. [26]

where P represents the plant of the system proposed, the z the alteration of the plant provoked by the external disturbance w, K represents the controller designed, u the effective control presented to the plant to begin the stabilization of the RLV and y which represents the final output of the system.

To calculate the plant P, the reasoning showed in [27] was followed: given the disturbance attenuation $\mu > 0$ the system Σ is considered *stabilizable* with the constant μ if there exists a controller capable of internally stabilizing it in the closed-loop system.

Furthermore, being the positive definite matrices Q, R, ζ and E - State Weighting Matrix, Control Weighting Matrix, Disturbance Matrix and Output Matrix, respectively - described as:

$$Q = Q_{intensity} * \begin{bmatrix} 1 & 0 & 0 & 0 & 0 & 0 \\ 0 & 1 & 0 & 0 & 0 & 0 \\ 0 & 0 & 1 & 0 & 0 & 0 \\ 0 & 0 & 0 & 1 & 0 & 0 \\ 0 & 0 & 0 & 0 & 1 & 0 \\ 0 & 0 & 0 & 0 & 0 & 1 \end{bmatrix} \tag{30}$$

$$R = 0.8 * \begin{bmatrix} 1 & 0 \\ 0 & 1 \end{bmatrix} \tag{31}$$

$$\zeta = \begin{bmatrix} 1 & 0 & 0 & 0 & 0 & 0 \\ 0 & 1 & 0 & 0 & 0 & 0 \\ 0 & 0 & 1 & 0 & 0 & 0 \\ 0 & 0 & 0 & 1 & 0 & 0 \\ 0 & 0 & 0 & 0 & 1 & 0 \\ 0 & 0 & 0 & 0 & 0 & 1 \end{bmatrix} \tag{32}$$

$$E = \begin{bmatrix} 0 & 1 & 0 & 0 & 0 & 0 \\ 0 & 0 & 1 & 0 & 0 & 0 \\ 1 & 0 & 0 & 0 & 0 & 0 \end{bmatrix} \tag{33}$$

and using the Algebraic Ricatti Equation - ARE:

$$PA + A'P - \frac{1}{\varepsilon}PBR^{-1}B'P + \frac{1}{\mu}P\zeta\zeta'P + \frac{1}{\mu}E'E + \varepsilon Q = 0 \tag{34}$$

with $\mu > 0$, the positive-definite solution P can be found as long as there exists a solution to this ARE in which $\varepsilon > 0$. In this case:

$$\mu = 100 \quad \varepsilon = 0.5 \tag{35}$$

If such conditions are satisfied, it is now possible to affirm that the system Σ is *stabilizable* with the disturbance attenuation μ [27]. Then, the controller matrix K described in fig. (4) can be calculated as:

$$K = \frac{-R^{-1}B'P}{2\varepsilon} \tag{36}$$

The $Q_{intensity}$ represents the fact that the matrix Q was, in this work, variable throughout time. This fact will be addressed and justified later, but generally, Q has a fixed value in control algorithms.

3. H_∞ Optimal Controller Results

With the system fully explained and the H_∞ set up, the time to test it's efficiency came. Considering w as the disturbance signal, the standard system with disturbance would be:

$$\Sigma(t) = \begin{cases} \dot{x}(t) = A(t)x(t) + B(t)u(t) + \zeta(t)w(t) \\ y(t) = E(t)x(t) \end{cases} \tag{37}$$

being w a matrix with the same dimensions as the matrix M and only composed by zeros, except for the columns representing the injection of disturbance into the system:

$$w = \begin{bmatrix} 0 & \dots & w_h(t_l) & \dots & w_h(t_n) & \dots & 0 \\ 0 & \dots & w_\phi(t_l) & \dots & w_\phi(t_n) & \dots & 0 \\ 0 & \dots & w_\theta(t_l) & \dots & w_\theta(t_n) & \dots & 0 \\ 0 & \dots & w_v(t_l) & \dots & w_v(t_n) & \dots & 0 \\ 0 & \dots & w_\gamma(t_l) & \dots & w_\gamma(t_n) & \dots & 0 \\ 0 & \dots & w_\psi(t_l) & \dots & w_\psi(t_n) & \dots & 0 \end{bmatrix} \tag{38}$$

being ”l” and ”n” representations of the time where the disturbance is being injected.

3.1 Graphics Obtained

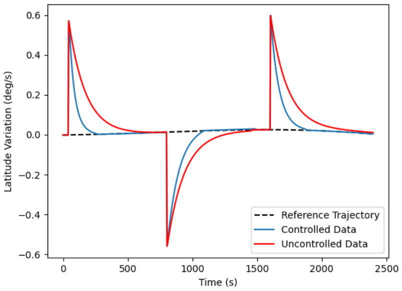

Figure 5. RLV's latitude variation development with three disturbances

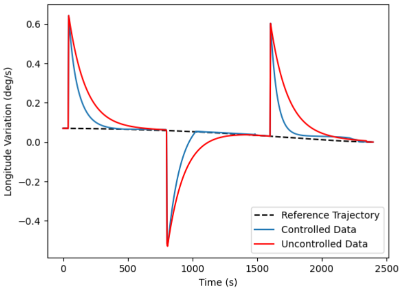

Figure 6. RLV's longitude variation development with three disturbances

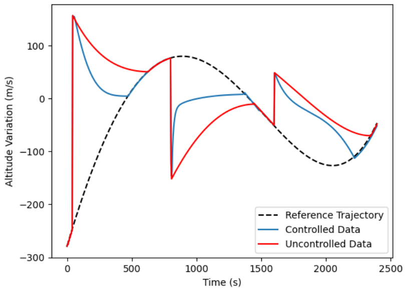

Figure 7. RLV's altitude development with three disturbances

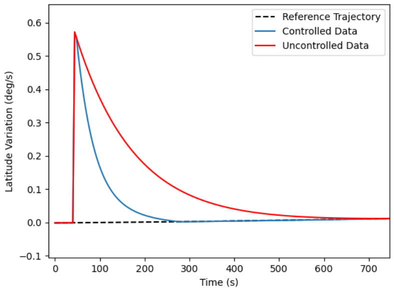

Figure 8. Close up to RLV's latitude development first disturbance

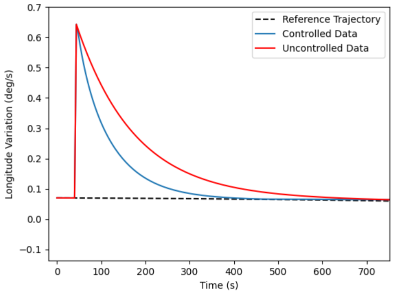

Figure 9. Close up to RLV's longitude development first disturbance

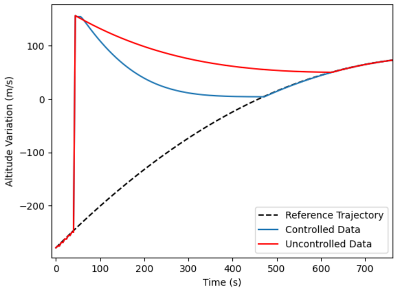

Figure 10. Close up to RLV's altitude development first disturbance

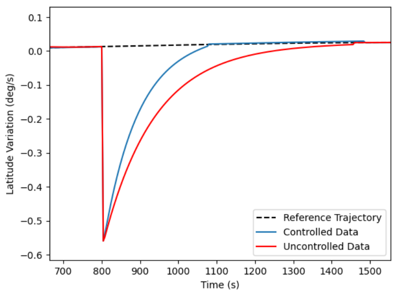

Figure 11. Close up to RLV's latitude development second disturbance

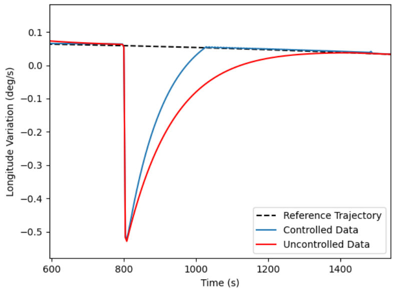

Figure 12. Close up to RLV's longitude development second disturbance

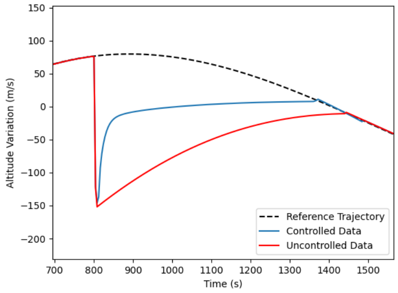

Figure 13. Close up to RLV's altitude development second disturbance

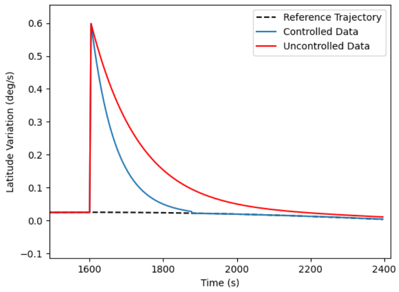

Figure 14. Close up to RLV's latitude development third disturbance

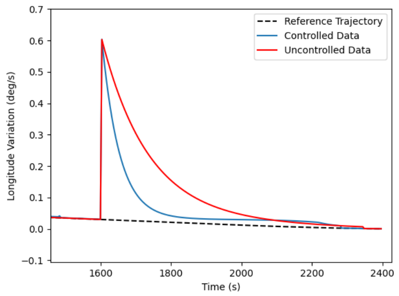

Figure 15. Close up to RLV's longitude development third disturbance

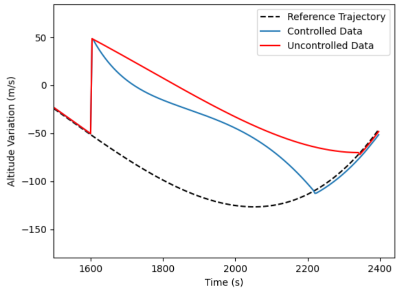

Figure 16. Close up to RLV's altitude development third disturbance

4. Conclusion

The H_∞ controller was successful in stabilizing the RLV's position variation throughout its descent. Furthermore, the controller was able to withstand several disturbances almost with no interval between the stabilization and the new disturbance and was capable of stabilizing each one through the vehicle's descent. This reveals the controller created in this paper is indeed a robust one, capable of correcting any disturbance provided to the system.

Acknowledgments

This research work was conducted in the Department of Aerospace Sciences of the University of Beira Interior, Portugal, and supported by the Aeronautics and Astronautics Research Group (AeroG) of the Associated Laboratory for Energy, Transports and Aeronautics (LAETA) of The Portuguese Foundation for Science and Technology (FCT).

References

[1] Nuno Patrício. *ESA* reúne-se em matosinhos para definir resposta a alterações climáticas e lixo espacial. *RTP Notícias*, 2021.

[2] Federal Aviation Administration. *Returning From Space: Re-entry*. U.S. Department of Transportation, 2011.

[3] Irwin E. Alber. *Aerospace Engineering on the Back of an Envelope*. ISBN: 978-3-642-22536-9. Springer, Praxis, 2003.

[4] Lt Col Kerry D-Hicks. *Introduction to Astrodynamic Reentry*. ISBN: 978-3-642-22536-9. Books Express Publishing, 2009.

[5] Jim Dumoulin. Mission events summary - information content from the nsts shuttle reference manual, 1998. https://science.ksc.nasa.gov/shuttle/technology/sts-newsref/sts_mes.html#mes_deorbit, Last Acessed on 2021-05-20.

[6] Nguyen X. Vinh, Adolf Busemann, and Robert D. Culp. *Hypersonic and planetary entry flight mechanics*. University of Michigan Press Ann Arbor, 1980.

[7] W. Hale, National Aeronautics, Space Administration, H. Lane, National Aeronautics, Space Administration (NASA) Staff, J. Young, Government Printing Office, K. Lulla, R. Crippen, and G. Chapline. *Wings In Orbit: Scientific and Engineering Legacies of the Space Shuttle 1971-2010*. NASA SP. NASA, 2010.

[8] Abdollah Homaifar Marwan Bikdash, Ken Sartor. Fuzzy guidance of the shuttle orbiter during atmospheric reentry. *Control Engineering Practice*, 3(7):295–303, 1999.

[9] Xiaoping Guo, Ruiyun Qi, and Xuelian Yao. Predictor-corrector guidance for reentry hypersonic vehicle based on feedback linearization. In *2017 29th Chinese Control And Decision Conference (CCDC)*, pages 6516–6521, 2017.

[10] Michael H. Breitner. Robust optimal on-board reentry guidance of an european space shuttle: Dynamic game approach and guidance synthesis via neural networks. *JOURNAL OF OPTIMIZATION THEORY AND APPLICATIONS*, 107:481–503, 07 2000.

[11] Yongji Wang Xing Wei, Lei Liu. Reentry trajectory optimization for a hypersonic vehicle based on an improved adaptive fireworks algorithm. *International Journal of Aerospace Engineering*, 2018.

[12] Gong Zifeng and Zhang et al. Hexin. Reentry tracking control of hypersonic glider based on legendre pseudospectral method. In *2018 Chinese Control And Decision Conference (CCDC)*, pages 1860–1864, 2018.

[13] Qiao Hao, Sun Peng, and Li Xinguo. General reentry trajectory planning method based on improved maneuver coefficient. *IEEE Access*, PP, 12 2018.

[14] Arunava Banerjee and M. Nabi. Re-entry trajectory optimization for space shuttle using sine-cosine algorithm. In *2017 8th International Conference on Recent Advances in Space Technologies (RAST)*, pages 73–77, 2017.

[15] Yifan Mao Lu. Wang, Qinghua Xing. Reentry trajectory rapid optimization for hypersonic vehicle satisfying waypoint and no-fly zone constraints. *Journal of Systems Engineering and Eletronics*, 26(6):1277–1290, 2015.

[16] Earth's spherical model. https://www.gratispng.com/png-tbkf6t/, Last Acessed on 2021-12-14.

[17] Davood Abbasi and Mahdi Mortazavi. A new concept for atmospheric reentry optimal guidance: An inverse problem inspired approach. *Mathematical Problems in Engineering*, 2013, 01 2013.

[18] Xiaoping Guo, Ruiyun Qi, and Xuelian Yao. Predictor-corrector guidance for reentry hypersonic vehicle based on feedback linearization. *International Journal of Aerospace Engineering*, pages 6516–6521, 2017.

[19] K. Bousson. Lecture notes of flight dynamics and control. Master's Degree of Aeronautical Engineering. Aerospace Sciences Department at University of Beira Interior, 2019.

[20] Aviation Performance Solutions. What is angle of attack? — three critical angles. https://www.apstraining.com/resource/three-critical-angles/, Last Acessed on 2021-06-10.

[21] R. C. et all Ried. Space shuttle orbiter entry heating and tps response: Sts-1 predictions and flight data. In *Langley Research Center Computational Aspects of Heat Transfer in Struct*, pages 327–348. NASA, 1982.

[22] John T. Betts. *6. Optimal Control Examples*. siam, 2010.

[23] Henrique Ferrolho. Space shuttle reentry trajectory. https://github.com/ferrolho/space-shuttle-reentry-trajectory, Last Acessed on 2021-06-20.

[24] Prof. Mireille E. Broucke. Linearization of nonlinear systems. 2007.

[25] Ximena Cubillos and Luiz Souza. Using of h-infinity control method in attitude control system of rigid-flexible satellite. *Mathematical Problems in Engineering*, 2009, 12 2009.

[26] P. Apkarian and Dominikus Noll. The H∞ Control Problem is Solved. *Aerospace Lab*, (13):pages 1–11, November 2017.

[27] P.P. Khargonekar, I.R. Petersen, and M.A. Rotea. H/sub infinity /-optimal control with state-feedback. *IEEE Transactions on Automatic Control*, 33(8):786–788, 1988.